# The RNF138 E3 ligase displaces Ku to promote DNA end resection and regulate DNA repair pathway choice

Ismail Hassan Ismail[1,2*], Jean-Philippe Gagné[3], Marie-Michelle Genois[3, 4], Hilmar Strickfaden[1], Darin McDonald[1], Zhizhong Xu[1], Guy G Poirier[3] , Jean-Yves Masson[3, 4] and Michael J Hendzel[1, *]

[1]Department of Oncology, Faculty of Medicine and Dentistry, University of Alberta, 11560 University Avenue, T6G 1Z2, Edmonton, Alberta, Canada. [2]Biophysics Department, Faculty of Science, Cairo University, 12613, Giza, Egypt. [3]CHU de Québec Research Center, CHUL Pavilion, Oncology Axis, 2705 boul. Laurier, Quebec city, Quebec, G1V 4G2, Canada. [4]Genome Stability Laboratory, CHU de Québec Research Center, HDQ Pavilion, Oncology Axis, 9 McMahon, Québec City, QC G1R 2J6, Canada. [4] Department of Molecular Biology, Medical Biochemistry and Pathology, Laval University, Québec City, QC G1V 0A6, Canada.

***Corresponding authors:**

Dr. Michael J Hendzel or Dr. Ismail Hassan Ismail
Department of Oncology,
Faculty of Medicine and Dentistry,
University of Alberta,
11560 University Avenue,
Edmonton, Alberta, Canada
E-mail: mhendzel@ualberta.ca
Tel: 1- 780-432-8439
Fax: 1- 780-432-8892

**Running title:** RNF138 promotes HR-mediated DNA double-strand break repair.

**Keywords:** Ubiquitylation, DNA end resection, Ku70/80, DNA repair, RNF138.

**DNA double-strand breaks (DSBs) are repaired mainly by non-homologous end joining (NHEJ) or homologous recombination (HR). Cell cycle stage and DNA end resection are believed to regulate the commitment to HR repair. Here we identify RNF138 as an ubiquitin E3 ligase that regulates the HR pathway. RNF138 is recruited to DNA damage sites through zinc fingers that have a strong preference for DNA with 5'- or 3'- single-stranded overhangs. RNF138 stimulates DNA end resection and promotes ATR-dependent signalling and DSB repair by HR, thereby contributing to cell survival upon exposure to DSB-inducing agents. Finally, we establish that RNF138-dependent Ku removal from DNA breaks is one mechanism whereby RNF138 can promote HR. These results establish RNF138 as an important regulator of DSB repair pathway choice.**

In mammalian cells, DNA double-strand breaks (DSBs) are repaired primarily by non-homologous end joining (NHEJ) and homologous recombination (HR)[1, 2]. NHEJ joins two DNA ends irrespective of their sequence, thereby generating errors if the two ends are unrelated or inaccurately processed[3]. Alternatively, DSBs can be joined via HR processes that typically use the sister chromatid as a template to restore sequence at the broken ends and execute error-free repair[4]. Canonical NHEJ involves the DNA-PKcs/Ku70/80-dependent ligation of broken DNA ends by DNA ligase IV. NHEJ is active throughout the cell cycle, but is most important during G1 prior to chromatid replication[5]. Conversely, HR occurs in the S and G2 phases of the cell cycle, when sister chromatids are available[6]. NHEJ is only active on minimally processed

DNA ends; it is inhibited by DNA end resection, the process by which 5′-3′ nucleolytic degradation generates single-stranded DNA (ssDNA). Initiation of DNA end resection by the CtIP/MRE11-RAD50-NBS1 (MRN) complex removes Ku from DNA ends to generate ssDNA overhangs that are refractory to canonical NHEJ[7, 8]. DNA end resection is a key step at which '*repair pathway choice*', the choice between NHEJ and HR, is determined because the generation of ssDNA would favor HR and concomitantly prevent the binding of NHEJ proteins[5, 9]. Extensive end resection is stimulated in the S and G2 phases of the cell cycle in a CDK1-dependent manner[10-12].

Cells lacking NHEJ genes reveal a DSB repair bias in favor of HR, suggesting that the two repair pathways can act on the same break[13]. The MRN complex has the ability to displace Ku from DNA ends in order to facilitate HR[7, 8]. However, if the MRN complex alone was sufficient to displace Ku from DNA ends, the high abundance and DSB binding of the MRN complex throughout the cell cycle could be problematic in G1, where NHEJ is preferred. Here we demonstrate that Nemo-like kinase (NLK)-associated ring finger protein (NARF) or RNF138 is an ubiquitin E3 ligase that regulates DNA end resection and HR and that this regulation involves direct interaction with and ubiquitylation of Ku80.

## Results

### Identification of RNF138 as a regulator of HR repair pathway

To identify novel factors required for HR-mediated DSB repair, we screened an siRNA library targeting putative members of the ubiquitin E3 ligase family in U2OS cells that stably co-express green fluorescent protein (GFP)-RAD52 and red fluorescent protein (RFP)- histone 2B (H2B) (**Fig. 1a**)[14]. We used GFP-RAD52 foci as an HR repair readout

in a microscopy–based screen to identify novel ubiquitin E3 ligases involved in HR repair. A RAD52 based reporter system was previously used to quantify the relative contribution of HR at different points of the cell cycle in single cells[15]. RAD52 is a recombinase mediator protein that forms foci at DSB sites that are committed to homology dependent repair[16]. RFP-H2B fluorescence was used to identify the cell nucleus. We predicted that depletion of an ubiquitin E3 ligase involved in HR repair would inhibit camptothecin (CPT)-induced GFP-RAD52 foci. CPT induces DSBs exclusively during DNA replication by trapping DNA topoisomerase 1 cleavage complexes and are mainly repaired through the HR repair pathway[17]. The lists of all targeted genes and the respective *Z*-scores (**Fig. 1b)** obtained in the screen are presented in **Supplementary Table 1**, and the list of 6 top-scoring genes ('hits') in U2OS cells is provided in **Fig. 1c**. The fact that the known DSB repair regulators RNF4, CtIP and BRCA1 scored prominently in our screen support the biological relevance of both our overall screening strategy and the additional top-scoring hits (**Fig. 1c**). One of the strongest hits in our screen was RNF138/NARF (**Fig. 1c and Supplementary Table 1**), whose down regulation impaired formation of RAD52 foci in cells exposed to CPT (**Fig. 1d**). In our screen, the impact of RNF138 knockdown on CPT-induced RAD52 focus formation was the most robust, almost as pronounced as the knockdown of CtIP and BRCA1, two major regulators of HR repair that have no known relationship to RNF138 and were used here as positive controls (**Fig. 1c-e**). To confirm these results, we examined the effect of RNF138 depletion on RAD51, a key regulator of HR repair, using immunofluorescence. RNF138 knock down impairs RAD51 foci formation, which is consistent with RNF138 being a positive regulator of HR pathway (**Fig. 1f**).

RNF138 is a poorly characterized ubiquitin E3 ligase that has a Ubiquitin Interacting Motif (UIM)-type ubiquitin-binding domain, the Really Interesting New Gene (RING) domain and C2HC and C2H2 zinc binding motifs (**Fig. 1g**)[18]. Orthologs of RNF138/NARF are found in most eukaryotes with the notable exception of yeast (**Supplementary Figure 1a**). Previous results are consistent with a role for RNF138/NARF in DNA repair. RNF138 contains a UIM-type ubiquitin-binding domain that belongs to the RAP80 family of UIM domains and is commonly found in DDR proteins[18]. Furthermore, RNF138 was phosphorylated upon DNA damage by ATM/ATR in a genome wide screen[19]. Thus, we set out to investigate the physiological relevance of these findings.

**RNF138 is recruited to sites of DNA damage**

We first determined whether RNF138 accumulates at DNA damage sites. Although we could not detect RNF138 recruitment to ionizing radiation induced foci (IRIF), we found that GFP-RNF138 is readily recruited to and retained at DNA damage sites after laser irradiation (**Fig. 2a**). Biochemical fractionation experiments show that a significant portion of RNF138 shifted from the soluble fraction to the chromatin fraction following IR (**Fig. 2b**). To extend our observations, we sought to determine whether RNF138 is recruited to a single DSB. We took advantage of a previously established DSB reporter system that uses *a LacI-FokI* nuclease fusion protein to create DSBs within a single genomic locus in U2OS cells (U2OS DSB reporter)[20]. Chromatin immunoprecipitation (ChIP) for RNF138 and γ-H2AX at the U2OS DSB reporter locus revealed several-fold enrichment of RNF138 and γ-H2AX upon

induction of DSBs by *Fok1* (**Fig. 2c**). These results demonstrate that DSBs can recruit RNF138.

**The recruitment of RNF138 to sites of DNA breaks is mediated by its zinc finger motifs**

We next wished to identify the region(s) within RNF138 that are important for its accumulation at DNA damage sites. We utilized a series of GFP-tagged RNF138 mutants (**Fig. 2d**) and monitored the recruitment of these mutants to sites of DNA damage. As shown in **Fig. 2e**, only the mutant RNF138 with the zinc fingers deleted (ΔZNF1-3) lost the ability to recruit to laser tracks, while wild-type (WT), the RING domain deletion mutant (ΔRING), the UIM domain deletion mutant (ΔUIM) and the single Zinc Finger domain mutants (ΔZNF1, ΔZNF2 and ΔZNF3) all retained at least some ability to bind at DNA damage sites (**Fig. 2e**). These observations suggest that the RNF138 ZNF domain, but not its E3 ligase activity, is essential for targeting RNF138 to DNA damage sites.

ZNF domains are capable of binding to poly (ADP-ribose) (PAR) polymers [21]. An *in vitro* PAR-binding assay was used to examine RNF138 binding to PAR polymers[22]. We found that RNF138 was unable to bind PAR (**Fig. 2f**). Under the same experimental conditions, histones (positive control) efficiently bind to PAR.

**RNF138 interacts with several DDR proteins upon genotoxic stress**

To explore how RNF138 might regulate the HR repair pathway, we generated a HEK293 cell line expressing a GFP-tagged RNF138 for the identification of potential RNF138-interacting proteins. Following GFP affinity purification, proteins associated with RNF138 were identified by mass spectrometry analysis (**Supplementary Table**

**2**). Interestingly, amongst these RNF138-associated proteins were DNA-PKcs, Ku70, and Ku80. We confirmed the interaction between RNF138 and Ku70/80 heterodimer. As shown in **Fig. 3a**, RNF138 interacted specifically with Ku80. Under the same conditions, RNF138 failed to interact with RNF8, a protein known to interact with Ku70/80. Reciprocally, Ku80 also specifically interacted with RNF138.

**RNF138 mediates Ku80 ubiquitylation following DNA damage**

RNF138 is an ubiquitin E3 ligase[23]. Therefore, we examined Ku80 ubiquitylation following DNA damage. We found that Ku80 is ubiquitylated and this ubiquitylation is stimulated upon IR, CPT and calichiamicin (CLM) treatments (**Fig. 3b**). This did not occur with DNA-damaging agents that do not directly yield DSBs (**Fig. 3b**). Furthermore, after siRNA-mediated depletion of RNF138, we found markedly reduced Ku80 ubiquitylation following DNA damage (**Fig. 3c**). Moreover, a catalytically inactive mutant (C18A/C54A, CA) as well as deletion of ZNF1-3 or RING domain of RNF138 abrogated the ability of RNF138 to ubiquitylate Ku80 *in vivo* (**Fig. 3d & e**). Additionally, both WT and the ΔZNF1-3 mutant of RNF138, but not the RING deletion mutant, bound to Ku80 (**Fig. 3f**). The RING domain of E3 ligases is involved in recruiting substrate to the E2 ligase[24]. Thus, this is consistent with RNF138 regulating ubiquitylation of Ku.

Previous reports suggested that RNF8 and FBXL12 mediate Ku ubiquitylation in response to DNA damage[25, 26]. We found that either RNF138 or RNF8 knockdown, but not FBXL12 knockdown, significantly reduced Ku ubiquitylation (**Fig. 3g**).

Given that RNF138 stimulates HR whereas RNF8 is reported to stimulate NHEJ, we next determined whether this reflected cell cycle-dependent differences in the ubiquitylation of Ku by RNF138 and RNF8. To purify G1 cells in cycling cultures, we took advantage of the Fucci system, which is based on fluorescent proteins with fragments of CDT1 and Geminin, for the G1 and S/G2 reporters, respectively. We subjected HeLa-Fucci cells to fluorescence-activated cell sorting (FACS) to purify G1 and S/G2 cells (**Supplementary Figure 1b)**. Analysis of cyclin A expression, which is restricted to S/G2 (**Supplementary Figure 1c**), indicated that we prepared a G1 cell fraction largely devoid of S/G2 cells. We found that DNA damage stimulates Ku80 ubiquitylation in G1 at levels similar to those of S/G2 and asynchronously dividing cells (**Fig. 3h**). Strikingly, we found that RNF138 depletion impairs Ku80 ubiquitylation only in S/G2 phase while it has no effect on G1 cells. In contrast, RNF8 abrogates Ku80 ubiquitylation in G1 but not in S/G2 phase of the cell cycle (**Fig. 3h**). Thus, our results suggest that RNF8 and RNF138 are the major ubiquitin E3 ligases responsible for Ku80 ubiquitylation but have non-redundant functions restricted to different parts of the cell cycle.

**RNF138-mediated Ku80 ubiquitylation regulates DSB repair choice**

The prevalent model for DSB repair pathway choice involves direct competition for binding between NHEJ (Ku70/Ku80) and HR (MRN/CtIP) determining the extent of DNA end resection, which inhibits NHEJ, to dictate pathway choice[5, 9]. The inhibition of HR (as measured by the reduction of RAD51 and RAD52 foci) and the observation that RNF138 interacts specifically with Ku heterodimers (**Supplementary Table 2**) led us to test the hypothesis that RNF138 stimulates Ku70/80 removal from the break sites

to bias repair towards HR. We used laser-induced DNA damage for the visualization of Ku80 accumulation at DNA damage sites. As previously reported, we observed immediate accumulation of Ku80 at damage sites after laser microirradiation (**Supplementary Figure 2a**). However, depletion of RNF138 markedly prolonged the retention of Ku80 at laser-induced DNA damage sites (**Supplementary Figure 2a**), implying that RNF138 is required for the removal of Ku80 from DSBs. When we blocked *de novo* Ku80 synthesis in cells with cycloheximide (CHX), the levels of Ku80 remained constant regardless of RNF138 expression status, suggesting that RNF138 does not target Ku80 to the proteasome-mediated degradation pathway (**Supplementary Figure 2b**). Consistent with the requirement of RNF138 for Ku80 turnover at DNA damage sites, RNF138 depleted cells showed a three-fold increase in NHEJ repair (**Supplementary Figure 2c**). Only reintroduction of WT RNF138, but not any of the ΔRING or ΔZNF1-3 deletion RNF138 mutants or catalytic dead (CA) mutant, was able to restore NHEJ capacity to normal levels (**Supplementary Figure 2c**). To further confirm these results, we asked whether or not RNF138-mediated Ku80 ubiquitylation influences the DNA binding capacity of Ku and hence its release from chromatin. We used immunoblotting to monitor the accumulation of Ku in soluble and chromatin fractions after treating cells with the radiomimetic drug CLM. Consistent with previous reports[27], treating cells with CLM immobilized Ku80 on damaged chromatin (**Supplementary Figure 3**). When cells were synchronized in G1, most of the ubiquitylated Ku80 is in the chromatin fraction upon DNA damage, whereas in S/G2, Ku80 ubiquitylation is mainly in the soluble fraction (**Supplementary Figure 3**). Interestingly, cellular depletion of RNF138 caused a persistence of Ku80 on damaged chromatin in S/G2 phase but had little effect on Ku80 retention in G1 phase.

Moreover, RNF138 depletion abolished Ku80 ubiquitylation only in S/G2.

To further confirm the above data, we compared the distribution of NBS1, RAD51, Mre11 and Ku80 relative to an *I-SceI*-induced DSB. Cells enriched in G1 or S/G2 phase (**Supplementary Figure 4**), with and without expression of RNF138, were induced for *I-SceI* site cleavage and analyzed by ChIP. When cells were synchronized in G1 phase of the cell cycle, I-SceI results in enrichment in Ku80 and RAD51 whereas Mre11 and NBS1 were not detected at the DSB sites **(Fig. 4a)**. When cells were synchronized for DSB formation in S/G2, Ku80 was not detected, whereas the levels of RAD51, NBS1 and Mre11 were substantially increased near the DSB. Depletion of RNF138 caused Ku persistence in S/G2 as well as suppressed RAD51 assembly in S/G2 but has no effect on Ku enrichment in G1 phase of the cell cycle **(Fig. 4a)**.

**RNF138 binds preferentially to ssDNA overhangs**

The data presented thus far indicated that Ku is retained at the DSB ends in the absence of RNF138, which might inhibit HR . We hypothesized that through its high affinity for DNA ends, Ku may rapidly bind to and protect DNA ends prior to end processing. The generation of short ssDNA overhangs by the Mre11 nuclease is then required to remove already bound Ku at DSB ends, thereby priming ends for CtIP/Exo1-dependent DNA end resection. Consistent with this notion, we found that Ku forms foci that partially overlapped with NBS1 at DSBs as early as 5 min after IR **(Fig. 4b)**. Nbs1 was used as a surrogate for Mre11 localization because the antibody gives better quality results in immunofluorescence experiments than Mre11 antibodies. Mre11 immunofluorescence showed similar results. Moreover, Ku80 foci form efficiently in cells synchronized in G1 and S/G2 phase of the cell cycle, suggesting

that the initial recruitment of Ku80 to sites of DNA damage is not dependent on cell cycle position **(Fig. 4b)**. Additionally, we found that CPT, which induces DSBs only in S phase, induces markedly less Ku foci per cell compared to IR and cellular depletion of RNF138 enhanced CPT-induced Ku foci that partially co-localized with NBS1 foci in S phase cells (**Supplementary Figure 5**). Addition of Mre11 nuclease inhibitor Mirin or ATM kinase inhibitor[28] did not inhibit but rather enhanced Ku80 foci, suggesting that Ku displacement from the sites of DNA damage is dependent on Mre11 and ATM activities (**Supplementary Figure 5**). Taken together, these data are consistent with an RNF138- and Mre11-dependent mechanism that actively displaces Ku from post replication-associated DSBs to commit cells to HR.

An attractive mechanism to couple RNF138-mediated ubiquitylation of Ku80 to Mre11 activity would be for the ZNF domains of RNF138 to bind selectively to the ssDNA overhangs generated by Mre11. We tested the ability of RNF138 ZNF domains to bind ssDNA overhang ends using an electrophoretic mobility shift assay (EMSA). WT RNF138, catalytically inactive RNF138 (C18A/C54A, CA) or RNF138 lacking ZNF1-3 domains were expressed in Sf9 cells, purified, and used for *in vitro* binding assays. Interestingly, we observed that WT RNF138 binds preferentially to double-stranded DNA (dsDNA) with 5'- tail or 3'-tails relative to ssDNA (**Fig. 5a-c**). Moreover, WT RNF138 bound poorly to blunt-ended dsDNA (**Fig. 5a**). Consistent with laser micro-irradiation experiments (**Fig. 2e**), RNF138 lacking ZNF1-3 was very inefficient (only 20% binding to ssDNA relative to WT) in binding to all DNA structures under the same conditions (**Fig. 5a**). These data demonstrate that, relative to blunt ends, RNF138 binds strongly to DNA ends containing ssDNA overhangs, supporting the hypothesis

that Mre11 nuclease-dependent processing of DSBs *in vivo* promotes RNF138 recruitment and DSB resection. Consistent with this, RNF138 depletion did not affect the recruitment of Mre11 to sites of DNA damage indicating that it has an activity in HR repair that is downstream of Mre11 loading (**Supplementary Figure 6a-c**). Moreover, treatment of cells with MRE11 specific siRNA or Mirin reduced the recruitment of RNF138 to sites of laser-induced DNA damage (**Supplementary Figure 7a-b**).

**RNF138 depletion inhibits DNA end resection**

HR is initiated by nucleolytic processing of the DSB ends to generate 3'-ssDNA tails that are initially coated by RPA[4, 29]. The requirements of ssDNA overhangs for RNF138 binding to DNA and the defects in RAD51 recruitment to damaged DNA in RNF138-depleted cells prompted us to examine the effect of RNF138 on DNA end resection. We monitored phosphorylation of the ssDNA binding protein RPA. DNA damage-induced phosphorylation of the RPA2 subunit on Ser-4 and Ser-8 was markedly reduced upon depletion of RNF138 (**Fig. 6a-b**). Importantly, we found that siRNA-mediated RNF138 depletion slightly decreased the S-phase population and increases the G2 population of cells (**Supplementary Figure 7c**). These results are consistent with previous findings in U251 cells, where knocking down RNF138 lessened the S and increased the G2 stage cells[30]. Thus, the impact of RNF138 depletion on RPA phosphorylation was not due to indirect cell cycle effects. Next, we sought to determine the impact of RNF138 on cellular sensitivity to different DNA damaging agents and observed that knockdown of RNF138 reduced colony formation of cells exposed to ionizing radiation (IR) or CPT (**Fig. 6c-d**). RNF138 depletion did not impair IR-induced focus formation

by the checkpoint mediator proteins MDC1 and 53BP1 (**Supplementary Figure 8a-b**). Furthermore, RNF138 depletion did not markedly affect phosphorylation of the ATM target Chk2 after IR or CPT treatment (**Fig. 6e-f**), thereby demonstrating that RNF138 is not crucial for ATM-dependent DNA damage signaling and checkpoint activation. In contrast, IR-induced and CPT-induced phosphorylation of Chk1, which is targeted by the ATM-related kinase ATR[31], was significantly impaired in RNF138-depleted cells (**Fig. 6e-f**). Furthermore, the RPA and Chk1 phosphorylation defects and the CPT hypersensitivity phenotype of RNF138-depleted cells were rescued by expression of an siRNA-resistant wild-type RNF138 construct (WT) but not by a mutant construct lacking the ability to localize to DNA damage sites (**Fig. 7a-b and Supplementary Figure 8b**). Additionally, accumulation of RPA at sites of CPT-induced damage and detection of ssDNA under non-denaturing conditions[32] was impaired in cells depleted of RNF138 (**Fig. 7c-f**).

To gain insight into how RNF138 contributes to DSB end resection, we examined whether its depletion affected the recruitment of various factors known to be involved in DNA end resection. Cells were laser microirradiated under conditions where DNA damage induced accumulation of DNA end resection proteins. While RNF138 depletion did not appreciably affect the formation of γ-H2AX at the DNA damage sites, CtIP, BLM and Exo1 recruitment to DNA damage sites were reduced in RNF138-depleted cells (**Fig. 7g-h and 8a-d**). Collectively, these results demonstrated that DNA end resection and subsequently recruitment of HR repair proteins to DSBs is attenuated following RNF138 depletion. Consistent with this, RNF138 depletion reduced the efficiency of HR by about 50% as measured by a chromosomal I-*SceI*-

mediated gene conversion assay (**Fig. 8e**,)[33]. Reintroduction of WT RNF138, but not of the CA, ΔRING or ΔZNF1-3 deletion RNF138 mutants, was able to rescue this HR repair deficiency (**Fig. 8e**). Collectively, the data suggest that, in mammalian cells, DSB ends must be free for DNA end resection to bias the DSB repair pathway choice towards HR-mediated repair. Consistent with this, pre-binding the DSB substrate with a Ku homolog from *Mycobacterium tuberculosis* that is not displaced from DSBs blocks Exo1-mediated DNA end resection *in vivo* and *in vitro*[34].

**Discussion**

HR is critical for error-free repair of DSBs and preservation of genome integrity. We have identified RNF138 as an ubiquitin E3 ligase that promotes HR and may do so, at least in part, by displacing Ku from the DSB. We found that RNF138 directly interacts with and promotes ubiquitylation of the Ku80 protein. Depletion of RNF138 enhanced cellular sensitivity to different DNA damaging agents, reduced RPA, CtIP, Exo1, and BLM recruitment to sites of DNA damage, and decreased HR repair. Thus, we have identified RNF138 as a previously undescribed but important regulatory component that acts at an early stage of the HR pathway preceding and required for extensive DNA end resection.

We found that RNF138 is recruited to sites of DSBs through its ZNF domains. Biochemically, ZNF domains are capable of binding to DNA, RNA and PAR. Consistent with this data, we demonstrated that RNF138 ZNFs contain a robust DNA binding activity that binds preferentially to resected dsDNA over ssDNA but does not bind blunt-ended dsDNA or PAR. Given that RNF138 acts at the early step of the HR pathway, the preferential ssDNA binding activity could shed some light on how

RNF138 promotes HR pathway. In this regard, it is possible that the MRN complex through its nuclease activity generates a short stretch of ssDNA overhang that acts as a priming signal for RNF138 to get recruited to sites of resected DSBs to displace Ku through ubiquitylation. Consistent with this, we found that RNF138 is downstream of Mre11 activity and RNF138-mediated Ku80 ubiquitylation decreased Ku binding to chromatin.

Accumulating evidence suggests that Ku should be removed from the DSB ends, as Ku trapped on DNA ends would preclude the assembly of HR factors at damage sites and hence HR repair[34-36]. RNF8 has previously been implicated in Ku removal[25]. We confirm that RNF8 is responsible for Ku80 ubiquitylation but this role is confined to G1, where HR is suppressed. RNF138 does not target Ku for proteasome-mediated degradation, unlike RNF8[25]. Most importantly, unlike RNF8, loss of RNF138 reduces HR and stimulates, rather than inhibits, NHEJ. Targeting Ku80 may not be the only mechanism whereby RNF138 stimulates end resection. In the accompanying paper by Schmidt *et al.*[37], UBE2D family ubiquitin E2 ligases were identified as the E2 partner of RNF138 in the regulation of HR and CtIP was identified as an RNF138 target. Thus, RNF138 may directly regulate end resection as well as the accessibility of the template to end resection machinery.

Based on our results, we propose a model for pathway choice in S/G2 phase (**Fig. 8f**). Following a DSB, Ku70/80 heterodimers and MRN complex are recruited to sites of DNA damage. Ku70/80 binds to DNA damage sites to protect the ends from non-specific processing. RNF138 then binds specifically to Mre11-resected DNA through its ZNF domains to remove Ku and enable CtIP/Exo1 nucleases recruitment to sites of DSBs for extensive resection and subsequent repair by HR.

RNF138-mediated Ku80 ubiquitylation is required for DNA end resection, for ATR-dependent signalling and DSB repair by HR. Our model assumes that DNA end protection by Ku occurs throughout the cell cycle and is independent of its role in NHEJ repair. This model postulates that if RNF138 is either inhibited or depleted in cells, Ku is not displaced, DNA end resection will be attenuated and HR will not occur.

## Acknowledgements

We thank Drs. Jermey Stark, Richard Baer, Susan M. Janicki, Ola Hammarsten, Roger Greenberg and Junjie Chen for providing valuable reagents. We thank Yan Coulombe, Marie-Christine Caron and Dr. Wael El Shemy for technical help. We also thank the Cellular Imaging Facility at the Cross Cancer Institute for the use of microscopes and image analysis software. The Proteomics Platform of the Quebec Genomics Center provided Mass spectrometry analysis. MJ Hendzel is an Alberta Innovates Health Solutions Senior Scholar. IH Ismail and Hilmar Strickfaden are recipients of the Alberta Cancer Foundation postdoctoral fellowships. M.M.G. was a CIHR Vanier scholar and is supported by a FRQS scholarchip; Guy G. Poirier holds a Tier 1 Canada Chair in Proteomics and J.Y.M. is a FRQS Chercheur National Investigator. This work was supported by grants from the Canadian Institute of Health Research (CIHR).

## Author Contributions

IHI conceived the study and did the majority of experiments. JPG and GP performed the mass spectrometry and PAR binding experiments. MMG and JYM did the DNA binding assays. ZH generated all DNA constructs and mutants in the study. DM performed some immunofluorescence experiments. HS generated the GFP-RAD52/RFP-H2B cells. IHI and MJH analyzed the data and wrote the manuscript. All authors discussed the work and manuscript.

## COMPETING FINANCIAL INTERESTS

The authors declare no competing financial interests.

Reprints and permissions information is available at www.nature.com/reprints.

## References


1. Hartlerode, A.J. & Scully, R. Mechanisms of double-strand break repair in somatic mammalian cells. *The Biochemical journal* **423**, 157-168 (2009).
2. Pardo, B., Gomez-Gonzalez, B. & Aguilera, A. DNA repair in mammalian cells: DNA double-strand break repair: how to fix a broken relationship. *Cellular and molecular life sciences : CMLS* **66**, 1039-1056 (2009).
3. Lieber, M.R. The mechanism of human nonhomologous DNA end joining. *The Journal of biological chemistry* **283**, 1-5 (2008).
4. San Filippo, J., Sung, P. & Klein, H. Mechanism of eukaryotic homologous recombination. *Annual review of biochemistry* **77**, 229-257 (2008).
5. Chapman, J.R., Taylor, M.R. & Boulton, S.J. Playing the end game: DNA double-strand break repair pathway choice. *Molecular cell* **47**, 497-510 (2012).
6. Rodrigue, A. *et al.* Interplay between human DNA repair proteins at a unique double-strand break in vivo. *The EMBO journal* **25**, 222-231 (2006).
7. Wu, D., Topper, L.M. & Wilson, T.E. Recruitment and dissociation of nonhomologous end joining proteins at a DNA double-strand break in Saccharomyces cerevisiae. *Genetics* **178**, 1237-1249 (2008).
8. Shim, E.Y. *et al.* Saccharomyces cerevisiae Mre11/Rad50/Xrs2 and Ku proteins regulate association of Exo1 and Dna2 with DNA breaks. *The EMBO journal* **29**, 3370-3380 (2010).
9. Symington, L.S. & Gautier, J. Double-strand break end resection and repair pathway choice. *Annual review of genetics* **45**, 247-271 (2011).
10. Jazayeri, A. *et al.* ATM- and cell cycle-dependent regulation of ATR in response to DNA double-strand breaks. *Nature cell biology* **8**, 37-45 (2006).
11. Aylon, Y., Liefshitz, B. & Kupiec, M. The CDK regulates repair of double-strand breaks by homologous recombination during the cell cycle. *The EMBO journal* **23**, 4868-4875 (2004).
12. Branzei, D. & Foiani, M. Regulation of DNA repair throughout the cell cycle. *Nature reviews. Molecular cell biology* **9**, 297-308 (2008).
13. Delacote, F., Han, M., Stamato, T.D., Jasin, M. & Lopez, B.S. An xrcc4 defect or Wortmannin stimulates homologous recombination specifically induced by double-strand breaks in mammalian cells. *Nucleic acids research* **30**, 3454-3463 (2002).
14. Li, W. *et al.* Genome-wide and functional annotation of human E3 ubiquitin ligases identifies MULAN, a mitochondrial E3 that regulates the organelle's dynamics and signaling. *PloS one* **3**, e1487 (2008).
15. Karanam, K., Kafri, R., Loewer, A. & Lahav, G. Quantitative live cell imaging reveals a gradual shift between DNA repair mechanisms and a maximal use of HR in mid S phase. *Molecular cell* **47**, 320-329 (2012).

16. Essers, J. *et al.* Nuclear dynamics of RAD52 group homologous recombination proteins in response to DNA damage. *The EMBO journal* **21**, 2030-2037 (2002).
17. Katyal, S. *et al.* Aberrant topoisomerase-1 DNA lesions are pathogenic in neurodegenerative genome instability syndromes. *Nature neuroscience* **17**, 813-821 (2014).
18. Giannini, A.L., Gao, Y. & Bijlmakers, M.J. T-cell regulator RNF125/TRAC-1 belongs to a novel family of ubiquitin ligases with zinc fingers and a ubiquitin-binding domain. *The Biochemical journal* **410**, 101-111 (2008).
19. Matsuoka, S. *et al.* ATM and ATR substrate analysis reveals extensive protein networks responsive to DNA damage. *Science* **316**, 1160-1166 (2007).
20. Shanbhag, N.M., Rafalska-Metcalf, I.U., Balane-Bolivar, C., Janicki, S.M. & Greenberg, R.A. ATM-dependent chromatin changes silence transcription in cis to DNA double-strand breaks. *Cell* **141**, 970-981 (2010).
21. Loughlin, F.E. & Mackay, J.P. Zinc fingers are known as domains for binding DNA and RNA. Do they also mediate protein-protein interactions? *IUBMB life* **58**, 731-733 (2006).
22. Ismail, I.H. *et al.* CBX4-mediated SUMO modification regulates BMI1 recruitment at sites of DNA damage. *Nucleic acids research* **40**, 5497-5510 (2012).
23. Yamada, M. *et al.* NARF, an nemo-like kinase (NLK)-associated ring finger protein regulates the ubiquitylation and degradation of T cell factor/lymphoid enhancer factor (TCF/LEF). *The Journal of biological chemistry* **281**, 20749-20760 (2006).
24. Ardley, H.C. & Robinson, P.A. E3 ubiquitin ligases. *Essays in biochemistry* **41**, 15-30 (2005).
25. Feng, L. & Chen, J. The E3 ligase RNF8 regulates KU80 removal and NHEJ repair. *Nature structural & molecular biology* **19**, 201-206 (2012).
26. Postow, L. *et al.* Ku80 removal from DNA through double strand break-induced ubiquitylation. *The Journal of cell biology* **182**, 467-479 (2008).
27. Cheng, Q. *et al.* Ku counteracts mobilization of PARP1 and MRN in chromatin damaged with DNA double-strand breaks. *Nucleic acids research* **39**, 9605-9619 (2011).
28. Britton, S., Coates, J. & Jackson, S.P. A new method for high-resolution imaging of Ku foci to decipher mechanisms of DNA double-strand break repair. *The Journal of cell biology* **202**, 579-595 (2013).
29. Bernstein, K.A. & Rothstein, R. At loose ends: resecting a double-strand break. *Cell* **137**, 807-810 (2009).
30. Zhou, Y.X. *et al.* A novel gene RNF138 expressed in human gliomas and its function in the glioma cell line U251. *Analytical cellular pathology* **35**, 167-178 (2012).
31. Cimprich, K.A. & Cortez, D. ATR: an essential regulator of genome integrity. *Nature reviews. Molecular cell biology* **9**, 616-627 (2008).
32. Raderschall, E., Golub, E.I. & Haaf, T. Nuclear foci of mammalian recombination proteins are located at single-stranded DNA regions formed after DNA damage. *Proceedings of the National Academy of Sciences of the United States of America* **96**, 1921-1926 (1999).

33. Pierce, A.J., Hu, P., Han, M., Ellis, N. & Jasin, M. Ku DNA end-binding protein modulates homologous repair of double-strand breaks in mammalian cells. *Genes & development* **15**, 3237-3242 (2001).
34. Shao, Z. *et al.* Persistently bound Ku at DNA ends attenuates DNA end resection and homologous recombination. *DNA repair* **11**, 310-316 (2012).
35. Frank-Vaillant, M. & Marcand, S. Transient stability of DNA ends allows nonhomologous end joining to precede homologous recombination. *Molecular cell* **10**, 1189-1199 (2002).
36. Kim, J.S. *et al.* Independent and sequential recruitment of NHEJ and HR factors to DNA damage sites in mammalian cells. *The Journal of cell biology* **170**, 341-347 (2005).
37. Christine K Schmidt, Y.G., Matylda Sczaniecka-Clift, Julia Coates, Satpal & Jhujh, M.D., Matthew Cornwell, Petra Beli and Stephen P Jackson Systematic E2 screening reveals a UBE2D-RNF138-CtIP axis
promoting DNA repair. *Nature cell biology* **In Press** (2015).

## Figure Legends

**Figure 1**. **Screening E3s for HR repair. (a)** A schematic depiction of the screening procedure combining custom siRNA arrays spanning 384 genes of the human ubiquitin E3 ligases and a readout based on monitoring the decrease of CPT-induced GFP-RAD52 foci **(b)** A scatterplot of Z-scores derived from the screen shown in (a). An average of at least 800-1200 cells were counted from two independent experiments. **(c)** List of the top six genes whose knockdown by siRNA decreased the formation of CPT-induced GFP- RAD52 foci. **(d)** Representative images from cells treated with the indicated siRNAs (2 independent experiments; one representative image shown). **(e)** Quantification of GFP-RAD52 foci formation after CPT treatment for 3 hrs. U2OS cells stably co-expressing GFP-RAD52 and RFP-H2B were either transfected with control siRNA (CTL siRNA) or one of two different siRNA against RNF138 (RNF138 siRNA1 and RNF138 siRNA2) for 48 hr. Cells were then treated with CPT for 3 hrs, fixed and imaged with a confocal microscope. Data show mean +/- s.d; n=800 cells, data pooled across two experiments. **(f)** RNF138 knock down impairs RAD51 foci formation. U2OS cells were either transfected with control siRNA (CTL siRNA) or one of two different siRNAs against RNF138 (RNF138 siRNA1 and RNF138 siRNA2) for 48 hrs. Cells were then treated with CPT for 1 hr. Immunostaining was done with the indicated antibodies (One representative image shown, the experiment was performed twice). Populations of cells with >5 RAD51 foci colocalized with γ H2AX were plotted by counting 100 cells per experiment on

the right panel. Data show mean +/- s.d; n=200 cells, data pooled across 2 experiments. **(g)** Modular architecture of human RNF138: RING (RING finger domain), ZNF1 (Zinc finger 1), ZNF2 (Zinc finger 2), ZNF3 (Zinc finger 3) and UIM (ubiquitin-interacting motif). Numbers indicate the amino acid numbers marking the domain boundaries. Scale bars are 5 μm.

**Figure 2. RNF138 is recruited to sites of DSBs through its ZNF domains.** **(a)** The fluorescence intensity of GFP–RNF138 at DNA damage sites is shown as a ratio relative to the unirradiated nucleoplasm and plotted versus time. Data show the means of two biologically independent experiments of 16 cells in each experiment. Representative pictures before and after DNA damage were shown on the right. **(b)** Enhanced binding of RNF138 to damaged chromatin in U2OS cells upon IR exposure (10 Gy for 60 min) analyzed by western blot with the indicated antibodies. **(c)** U2OS cells stably expressing the reporter locus were transfected with wild-type Fok1 (FOK1 WT) or Fok1 catalytically inactive mutant (FOK1 mut) endonuclease constructs. ChIP was performed with IgG, RNF138 and γ-H2AX antibodies. Quantitative PCR was performed and the Fok-1 DSB-induced enrichment for each primer and antibody is plotted. Data represent mean of two independent experiments; each sample in each experiment was run in triplicate. **(d)** Schematic representation of RNF138 deletion constructs used in Fig. 2e. **(e)** Recruitment of GFP-RNF138 or the individual GFP-tagged RNF138 deletion constructs to sites of laser-induced DNA damage after micro-irradiation in U2OS cells. Arrowheads highlight micro-irradiated regions. Top: Western blot analysis of U2OS cells expressing

GFP-RNF138 WT and GFP-RNF138 deletion mutants used in Fig. 2e. **(f)** *In vitro* PAR-binding assay. 1 μg of purified 6X-His-RNF138, BSA (negative control) or histones (positive control) was slot-blotted onto a nitrocellulose membrane, incubated with a TBS-T solution containing 250 nM of $^{32}$P-labeled PAR and developed by autoradiography. Unprocessed original scans of blots are shown in Supplementary Figure 9. Scale bars are 5 μm.

**Figure 3. RNF138 regulates Ku80 ubiquitylation in response to DNA damage. (a)** Reciprocal coimmunoprecipitation of endogenous RNF138 and Ku80 from HeLa cell extracts. Immunoprecipitation experiments were performed with cell extracts prepared in the presence of Benzonase®, which digests nucleic acids, to eliminate any potential indirect interaction via DNA. RNF8 was used as a known Ku interacting protein and hence as a positive control. FT: flow-through, EL: eluted proteins **(b)** Ku ubiquitylation occurs after agents that directly induce DSBs. *In vivo* ubiquitylation was performed as outlined in material and methods. Untreated (CTL) or treated with 1 nM calicheamicin (CLM), ionizing radiation (IR, 10 Gy), 250 J/m$^2$ UV, 100 μM hydrogen peroxide ($H_2O_2$), 1 μM camptothecin (CPT), and collected 1h post treatment. **(C)** RNF138 ubiquitylates Ku80 *in vivo* in response to DNA damage. HeLa cells were transfected with expression constructs encoding GFP-tagged ubiquitin (Ub) or GFP-Ku80 and Control siRNA (CTL siRNA) or one of two different RNF138 siRNAs (RNF138 siRNA1 and RNF138 siRNA2). Cells were exposed to IR (6 Gy) for 1 hr and immunoprecipitated and immunoblotted as indicated. **(d)** Cells were treated as in **(C)** except that cells were reconstituted with siRNA resistant WT RNF138

construct or RNF138 constructs lacking ZNF1-3 (ΔZNF1-3) or RING domain (ΔRING). **(e)** Cells were treated as in **(C)** except that they were reconstituted with siRNA resistant WT RNF138 construct or catalytic inactive RNF138 construct (CA). **(f)** Mapping out the RNF138 domain required for Ku80 interaction. HEK293 cells were transfected with different GFP-RNF138 truncation mutants and extracts were subjected to GFP or Ku80 immunoprecipitation and immunoblotted as indicated. **(g)** Cells were either transfected with either control siRNA (CTL) or siRNA against RNF138, RNF8 or FBXL12. DNA damage was induced by CLM and immunoprecipitation experiments were performed as indicated. **(h)** Fucci cells were either transfected with control siRNA (CTL siRNA) or siRNAs against RNF138 (RNF138 siRNA) or RNF8 (RNF8 siRNA). Asynchronous (Asy), S/G2 or G1 cells were sorted by flow cytometry and exposed or not exposed to IR. Immunoprecipitation and immunoblots were done as indicated. Unprocessed original scans of blots are shown in Supplementary Figure 9.

**Figure 4. ChIP of endogenous RAD51, NBS1, Ku80 and MRE11 on a unique DSB.**

**(a)** The presence of the proteins was verified during the G1 or S/G2 phase of the cell cycle. Real-time PCR on ChIP samples were carried out at three primer positions 94–378, 675–1044 and 901–1210 nucleotides from the break. Fold-enrichment represents the enrichment of the proteins compared to an IgG control (normalized with a PCR internal control to a locus other than the DSB). Data represent mean of two independent experiments; each sample was run in triplicate. **(b)** Immunostaining of Hela cells synchronized either in G1 or S/G2

phase of cell cycle. Cells were irradiated with 10 Gy of IR and then allowed to recover for 5 min before RNAase extraction as described in the Materials and Methods. Cells were fixed and stained as indicated. Images were captured using Z-stacks, deconvolved using Hygens deconvolution software and Ku80 foci were quantified using MetaXpress® Software. Average Ku80 foci per cell were counted from two independent experiments and plotted as indicated. Data show mean +/- s.d; n=30 cells, data pooled across two experiments. Scale bars are 10 μm.

**Figure 5. Purification and DNA binding activity of RNF138. (a)** Left: SDS-PAGE of purified RNF138 proteins. Purified proteins (150 ng) were loaded on a 15% SDS-PAGE, and stained with coomassie blue. Lane 1, molecular weight markers (Bio-Rad); lane 2, purified WT RNF138; lane 3, purified catalytic mutant C18A/C54A RNF138; lane 4, purified DNA binding mutant RNF138 ΔZNF1-3. Middle: DNA binding activity of RNF138. RNF138 WT (200 nM) (lane 2) and C18A/C54A RNF138 (200 nM) (lane 3) preferentially bind single-strand DNA over double-strand DNA (compare top (single stranded DNA) and bottom blot (dsDNA)) while RNF138 ΔZNF1-3 (200nM) (lane 4) exhibits low DNA binding activity. The arrowhead indicates the protein-DNA complex. Quantification of the blots in the middle is shown on the right. Data show mean +/- s.d; n=3, data pooled across three independent experiments. **(b&C)** Competition EMSA with RNF138. WT and catalytic mutant proteins preferentially bind tailed DNA over single-strand DNA. A mixture of ssDNA and tailed DNA was incubated together with increasing concentration (0-200 nM) of RNF138 WT (lane 2-4), C18A/C54A RNF138 (lane 5-7) and RNF138 ΔZNF1-3 (lane 8-10). **(b)** 3'-tail or

**(c)** 5'-tail. Quantification of the blots in the middle is shown on the right of each panel**.** The arrowheads indicate the protein-DNA complex. Data show mean +/- s.d; n=3independent experiments. Unprocessed original scans of blots are shown in Supplementary Figure 9.

**Figure 6. RNF138 knock down results in hypersensitivity to DSB-inducing agents and impairs ATR-dependent signalling. (a)** Western blot analysis of RPA phosphorylation (p-RPA S4/8) 90 min after CPT treatment (+CPT) on whole cell extracts from U2OS cells treated with the indicated siRNAs (CTL: control) or one of two different RNF138 siRNAs (RNF138 siRNA1 and RFN138 siRNA2). Cyclin A levels monitor the presence S/G2 cells and tubulin is used as loading control. **(b)** Immunodetection of phosphorylated RPA (p-RPA S4/8) at laser microirradiation sites in U2OS cells treated with the indicated siRNAs. U2OS cells were exposed to laser micro-irradiation and immunostained as indicated. The proportion of cells with p-RPA stripes positive with γ-H2AX stripes were plotted by counting at least 35 cells per experiment on the right panel. Error bars represent mean +/- sd of n=3 independent experiments. 120 cells were evaluated in total. **(c&d)** Clonogenic survival of U2OS cells upon RNF138 depletion (RNF138 siRNA1 and RNF138 siRNA2) compared to control (CTL siRNA) after treatment with the indicated agents. Cell survival in response to: **(c)** IR and **(d)** CPT. Error bars represent SEM from n=3 biological experiments. **(e,f)** Phosphorylation of proteins upon RNF138 depletion with two different siRNAs (RNF138 siRNA1 and RNF138 siRNA2) analyzed by western blotting of

U2OS whole cell extracts at the indicated times after cell exposure to 4 Gy IR **(e)** or 1 μM CPT **(f)**. Scale bars are 5 μm.

**Figure 7. RNF138 acts at the early step of the HR pathway and is upstream of CtIP. (a)** Western blotting of total extracts from U2OS cells transfected with the indicated siRNAs and plasmids (vector alone or RNF138-encoding plasmids) after exposure to 1 μM CPT for 1 hr. CTL: control siRNA; RNF138 siRNA1 is an siRNA that targets the RNF138 3'UTR. **(b)** Clonogenic survival of U2OS cells transfected as in (a) in response to CPT. Error bars represent SEM from n=3 biological experiments. **(c)** Recruitment of RPA to sites of CPT-induced DNA damage in cells depleted of RNF138 with two different siRNA (RNF138 siRNA1 and RNF138 siRNA2) compared to controls (CTL). Cells were fixed 1 hr after CPT treatment. **(d)** Quantification of data shown in **c**. The proportion of cells with >10 RPA foci in γ-H2AX positive cells were calculated by counting 100 γ-H2AX positive cells per experiment. Data show the mean+/- SD of n=200 cells, data pooled across two biologically independent experiments. Western blot analysis of cells to estimate the knock down efficiency of RNF138 is shown on the right and served as a control. **(e)** Effect of RNF138 depletion on ssDNA (BrdU signal) formation using two different siRNAs (RNF138 siRNA1 and RNF138 siRNA2) compared to controls (CTL) after IR exposure is shown. **(f)** Quantification of data shown in **e**. Population of cells with >10 BrdU foci in γ-H2AX positive cells were calculated by counting 100 γ-H2AX positive cells per experiment. Data show the mean+/- SD of n=200 cells, data pooled across two independent experiments. **(g)** Recruitment of GFP-BLM to sites of laser-

induced DNA damage in cells depleted of RNF138 (RNF138 siRNA1 and RNF138 siRNA2) compared to controls (CTL). Cells were fixed 1 hr after microirradiation. Arrowheads highlight microirradiated regions. **(h)** The proportion of cells with BLM stripes positive with γ H2AX stripes were plotted by counting at least 45 cells per experiment on the right panel. Data show the mean+/- SD of n=112 cells, data pooled across two biologically independent experiments. Unprocessed original scans of blots are shown in Supplementary Figure 9. Scale bars are 5 μm.

**Figure 8. RNF138 regulates DNA end resection. (a-d)** Recruitment of Exo1 or CtIP to sites of laser-induced DNA damage in cells depleted of RNF138 (RNF138 siRNA1 and RNF138 siRNA2) compared to controls (CTL); cells were fixed 1 hr after microirradiation. Two independent experiments; at least 52 cells were laser irradiated per experiment, 1 representative experiment shown in a and c. Histograms showing the percentage of γ-H2AX-positive stripes in control siRNA or RNF138 siRNA-treated cells that were stained with Exo1 (**b**) or CtIP (**d**) antibody, respectively. Data show the mean +/- SD of **b** (n=54) or **d** (n= 62 cells, data pooled across two biologically independent experiments. (**e**) HR-mediated gene conversion assay. HR efficiencies are normalized to CTL. Data show the mean +/- SD of n=3 biologically independent experiments. Approximately 20,000 cells were evaluated by flow cytometry in each experiment. CtIP depletion is used as a positive control. siRNA efficiencies are shown on the western blot panel (bottom). (**f**) Proposed model for the function of RNF138 in regulating the choice of DSB repair pathway. Following DSB

induction in cells, the MRN complex and Ku70/80 bind independently to the DNA damage site to protect the ends from non-specific processing. In S-and G2 phase, Mre11 nuclease resects DSB to create short DNA overhangs. The ssDNA is recognized by the zinc fingers of RNF138, loading this ubiquitin E3 ligase onto the minimally resected DNA. Ku is then actively displaced from the DSB following RNF138-dependent ubiquitylation. The removal of Ku allows the CtIP/Exo1 nucleases are recruited to extensively resect the DSB, committing the break to HR repair. RNF138-mediated ubiquitylation is thereby required for DNA end resection, for ATR-dependent signalling and DSB repair by HR. Unprocessed original scans of blots are shown in Supplementary Figure 9. Scale bars are 5 μm.

A

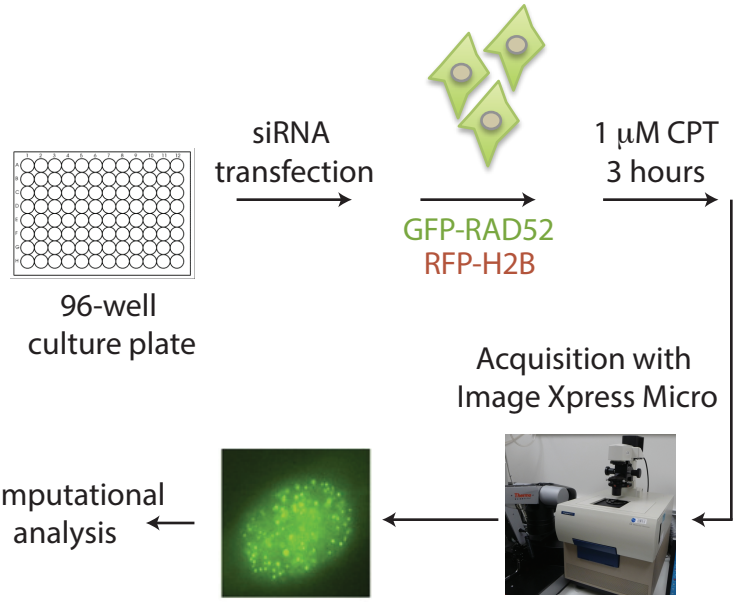


B

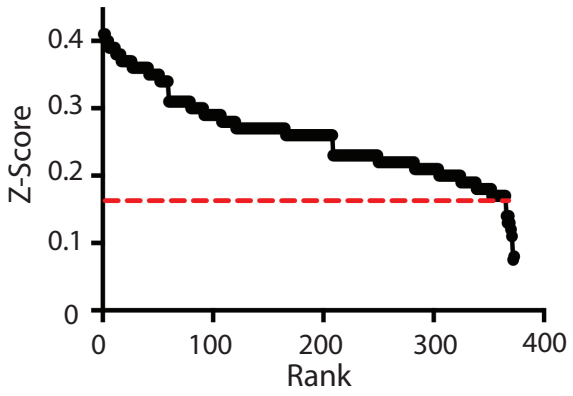


C

| Gene name | Gene symbol | Average Z-score |
|---|---|---|
| S-phase kinase-associated protein 2 | SKP2 | 0.14 |
| Stem cell factor | SCF | 0.13 |
| RING finger protein 4 | RNF4 | 0.12 |
| Breast cancer type 1 susceptibility protein | BRCA1 | 0.11 |
| Nemo-like kinase-associated RING finger protein | NARF/RNF138 | 0.075 |
| DNA endonuclease RBBP8 | CtIP | 0.06 |

D

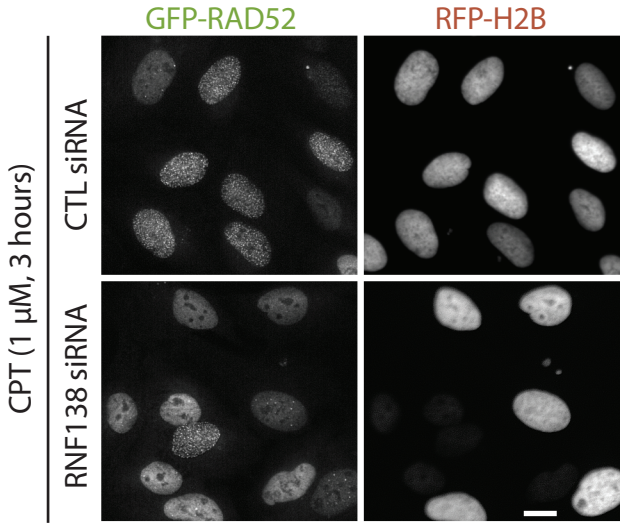


E

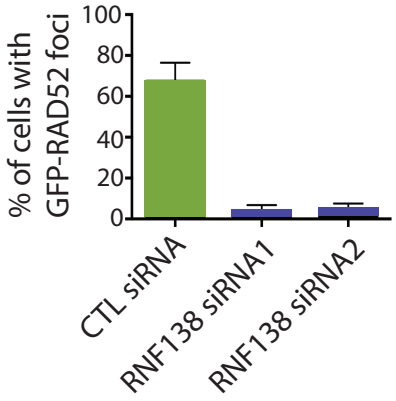


F

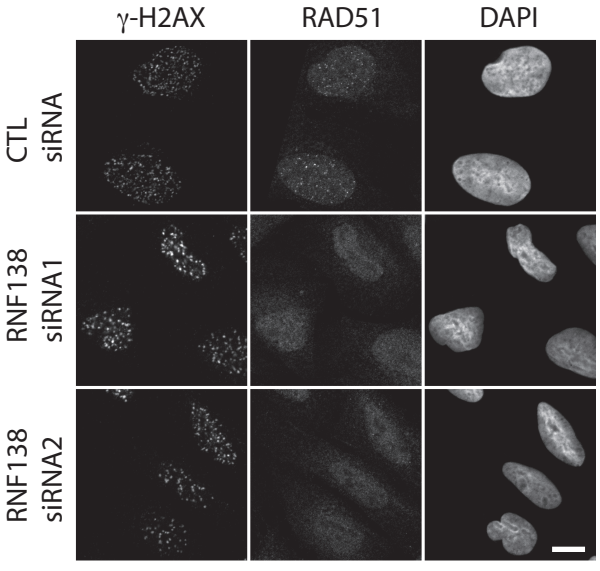


G

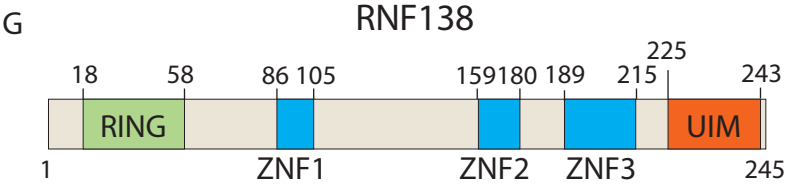


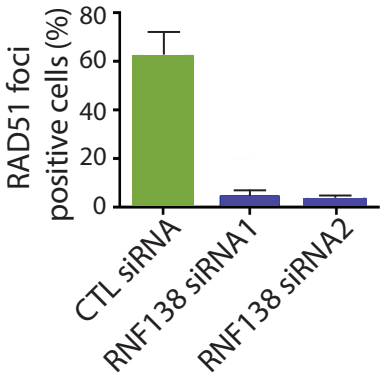

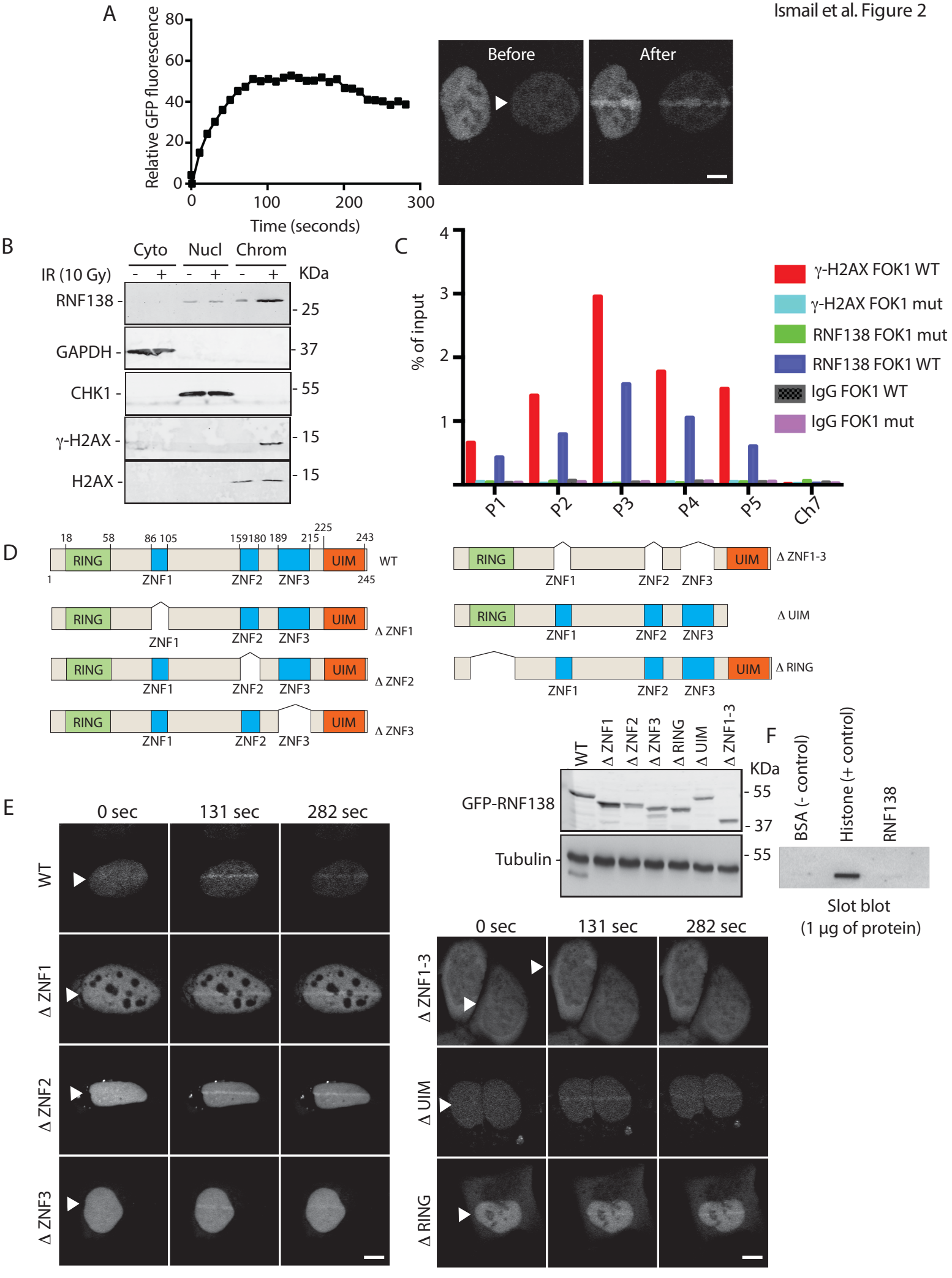
A
Relative GFP fluorescence
Time (seconds)
Before
After
B
Cyto
Nucl
Chrom
IR (10 Gy)
KDa
RNF138
GAPDH
CHK1
γ-H2AX
H2AX
C
% of input
γ-H2AX FOK1 WT
γ-H2AX FOK1 mut
RNF138 FOK1 mut
RNF138 FOK1 WT
IgG FOK1 WT
IgG FOK1 mut
P1
P2
P3
P4
P5
Ch7
D
RING
ZNF1
ZNF2
ZNF3
UIM
WT
Δ ZNF1
Δ ZNF2
Δ ZNF3
Δ ZNF1-3
Δ UIM
Δ RING
E
0 sec
131 sec
282 sec
WT
Δ ZNF1
Δ ZNF2
Δ ZNF3
Δ ZNF1-3
Δ UIM
Δ RING
F
GFP-RNF138
Tubulin
KDa
BSA (- control)
Histone (+ control)
RNF138
Slot blot
(1 µg of protein)

Ismail et al. Figure 3

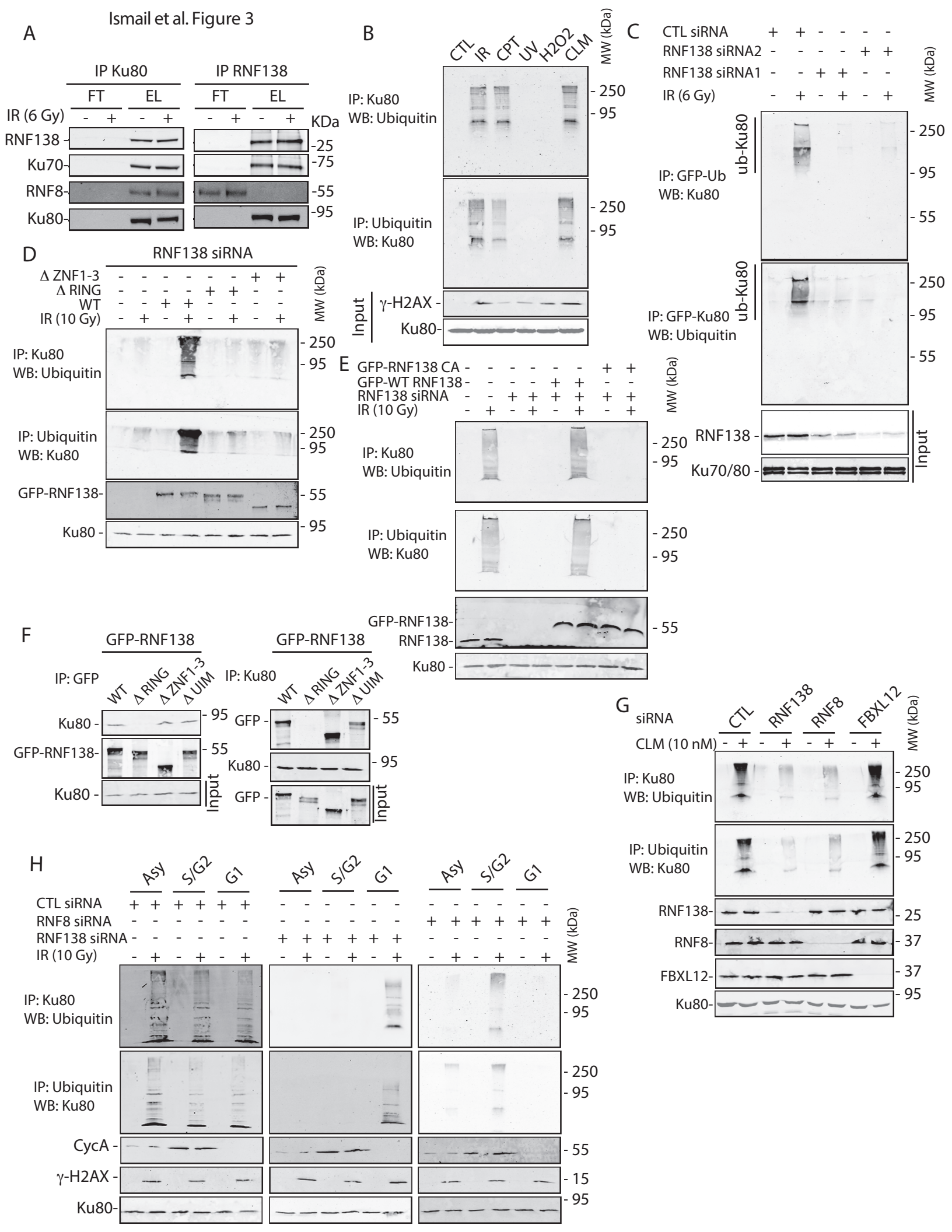

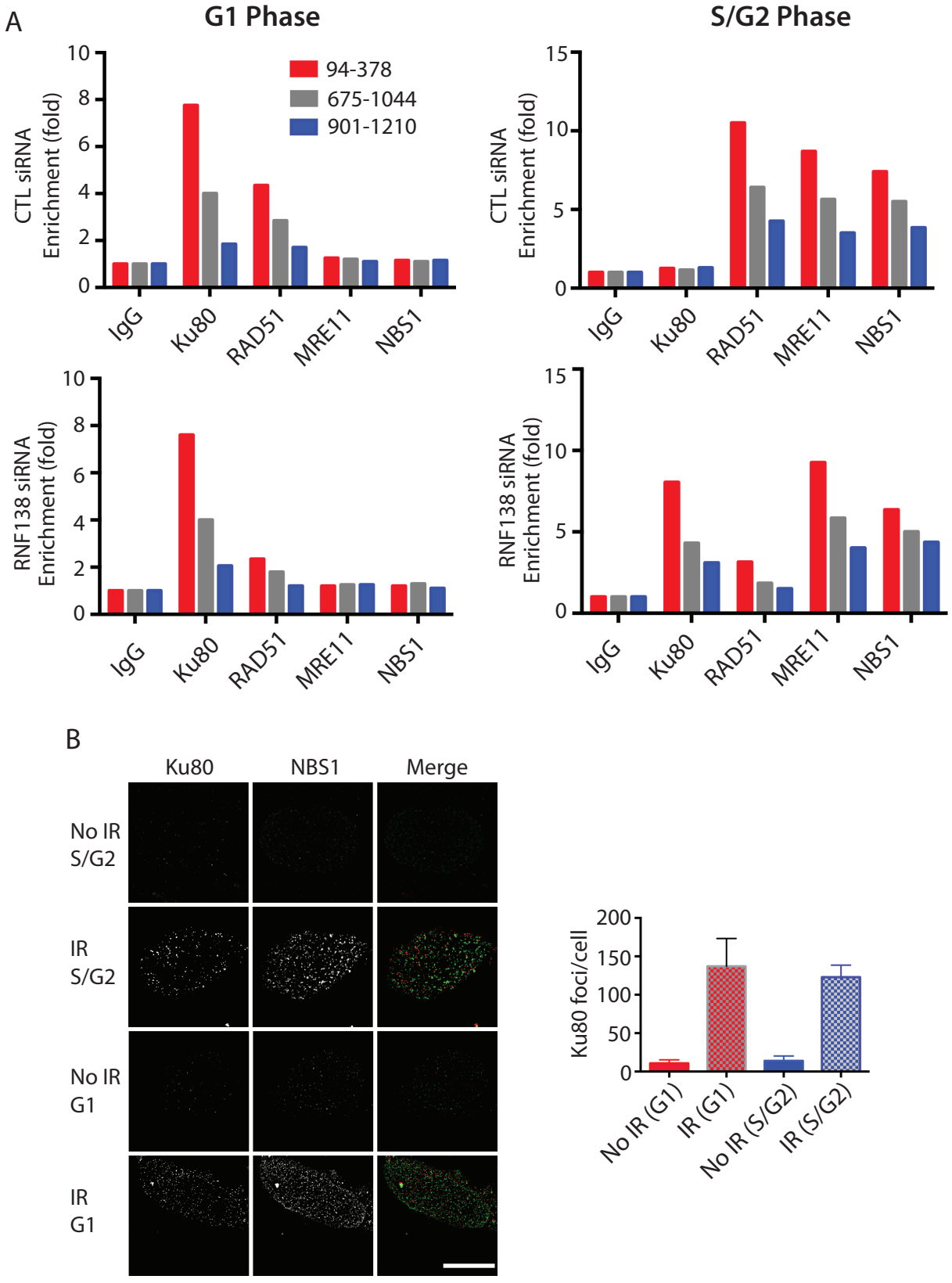
A
G1 Phase
S/G2 Phase
94-378
675-1044
901-1210
CTL siRNA Enrichment (fold)
RNF138 siRNA Enrichment (fold)
IgG
Ku80
RAD51
MRE11
NBS1
B
Ku80
NBS1
Merge
No IR S/G2
IR S/G2
No IR G1
IR G1
Ku80 foci/cell
No IR (G1)
IR (G1)
No IR (S/G2)
IR (S/G2)

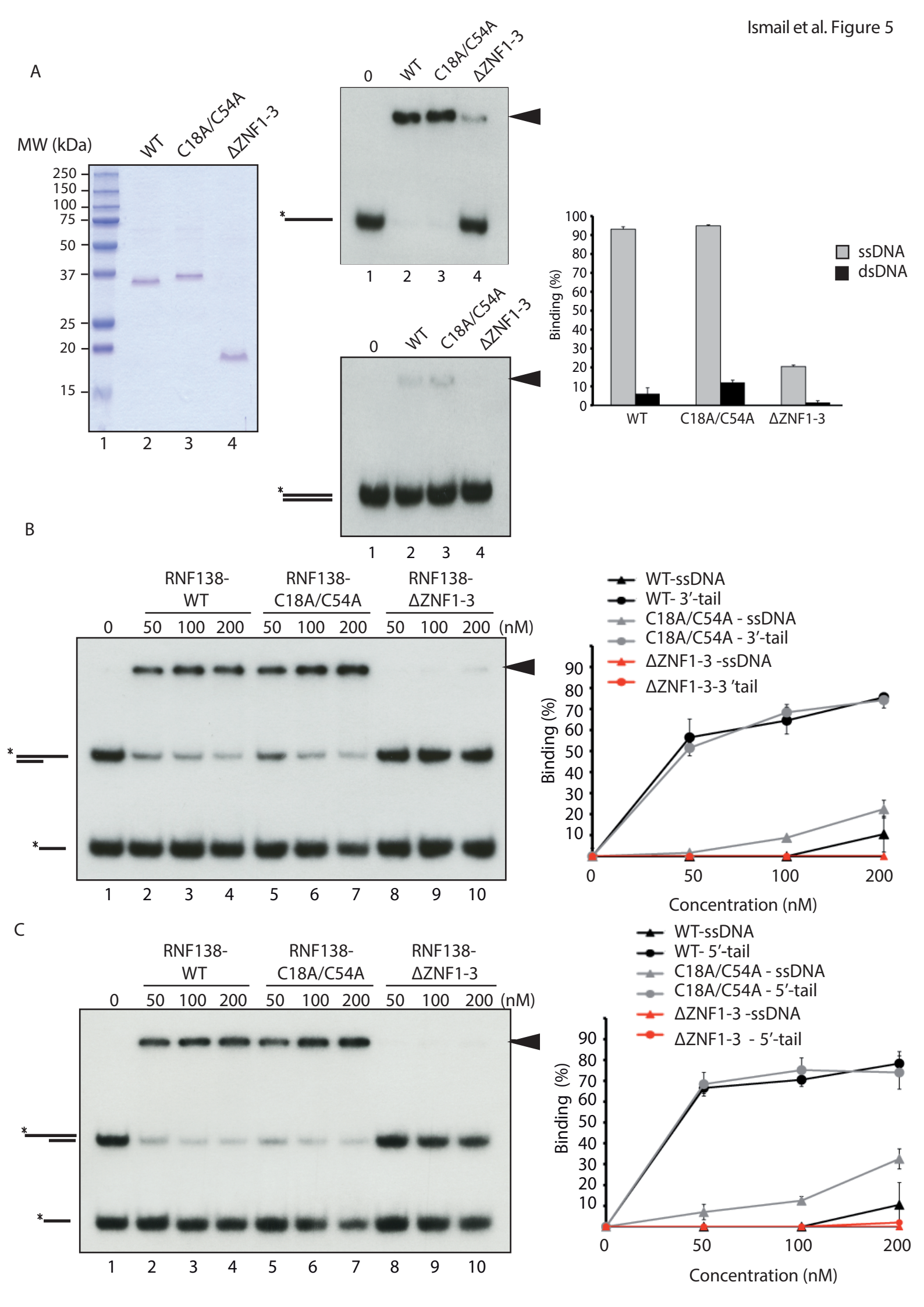
A
MW (kDa)
WT
C18A/C54A
ΔZNF1-3
250
150
100
75
50
37
25
20
15
1 2 3 4
0
WT
C18A/C54A
ΔZNF1-3
*
1 2 3 4
0
WT
C18A/C54A
ΔZNF1-3
*
1 2 3 4
Binding (%)
100
90
80
70
60
50
40
30
20
10
0
WT
C18A/C54A
ΔZNF1-3
ssDNA
dsDNA
B
RNF138-WT
RNF138-C18A/C54A
RNF138-ΔZNF1-3
0 50 100 200 50 100 200 50 100 200 (nM)
*
*
1 2 3 4 5 6 7 8 9 10
WT-ssDNA
WT- 3′-tail
C18A/C54A - ssDNA
C18A/C54A - 3′-tail
ΔZNF1-3 -ssDNA
ΔZNF1-3-3 ′tail
Binding (%)
90
80
70
60
50
40
30
20
10
0
50
100
200
Concentration (nM)
C
RNF138-WT
RNF138-C18A/C54A
RNF138-ΔZNF1-3
0 50 100 200 50 100 200 50 100 200 (nM)
*
*
1 2 3 4 5 6 7 8 9 10
WT-ssDNA
WT- 5′-tail
C18A/C54A - ssDNA
C18A/C54A - 5′-tail
ΔZNF1-3 -ssDNA
ΔZNF1-3 - 5′-tail
Binding (%)
90
80
70
60
50
40
30
20
10
0
50
100
200
Concentration (nM)

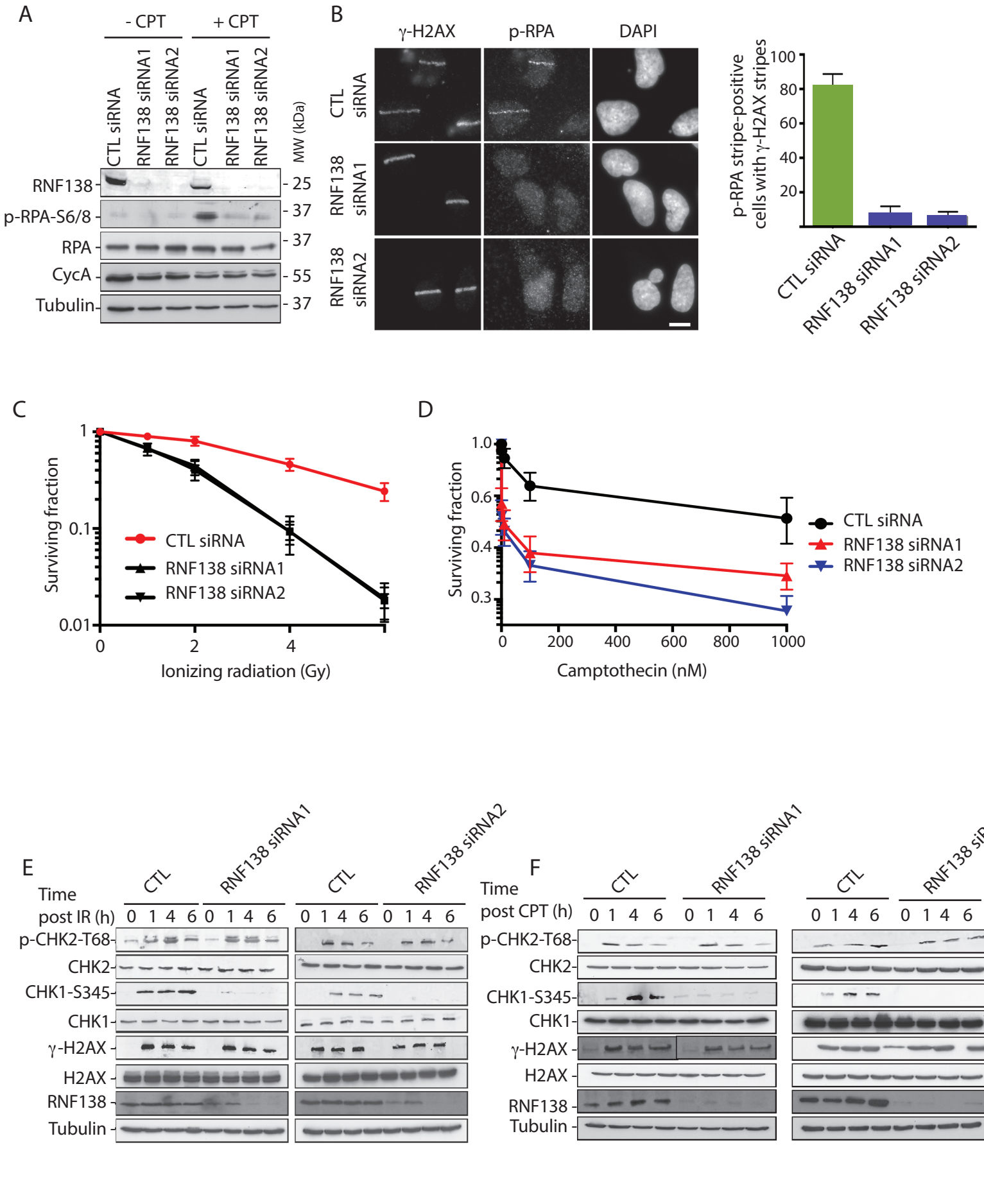
A
- CPT
+ CPT
CTL siRNA
RNF138 siRNA1
RNF138 siRNA2
CTL siRNA
RNF138 siRNA1
RNF138 siRNA2
MW (kDa)
RNF138
p-RPA-S6/8
RPA
CycA
Tubulin
25
37
37
55
37
B
γ-H2AX
p-RPA
DAPI
CTL siRNA
RNF138 siRNA1
RNF138 siRNA2
p-RPA stripe-positive cells with γ-H2AX stripes
100
80
60
40
20
CTL siRNA
RNF138 siRNA1
RNF138 siRNA2
C
Surviving fraction
1
0.1
0.01
CTL siRNA
RNF138 siRNA1
RNF138 siRNA2
0
2
4
Ionizing radiation (Gy)
D
Surviving fraction
1.0
0.6
0.4
0.3
0
200
400
600
800
1000
Camptothecin (nM)
CTL siRNA
RNF138 siRNA1
RNF138 siRNA2
E
Time post IR (h)
CTL
RNF138 siRNA1
CTL
RNF138 siRNA2
0 1 4 6 0 1 4 6 0 1 4 6 0 1 4 6
p-CHK2-T68
CHK2
CHK1-S345
CHK1
γ-H2AX
H2AX
RNF138
Tubulin
F
Time post CPT (h)
CTL
RNF138 siRNA1
CTL
RNF138 siRNA2
0 1 4 6 0 1 4 6 0 1 4 6 0 1 4 6
MW (kDa)
p-CHK2-T68
CHK2
CHK1-S345
CHK1
γ-H2AX
H2AX
RNF138
Tubulin
55
55
55
55
15
15
25
37

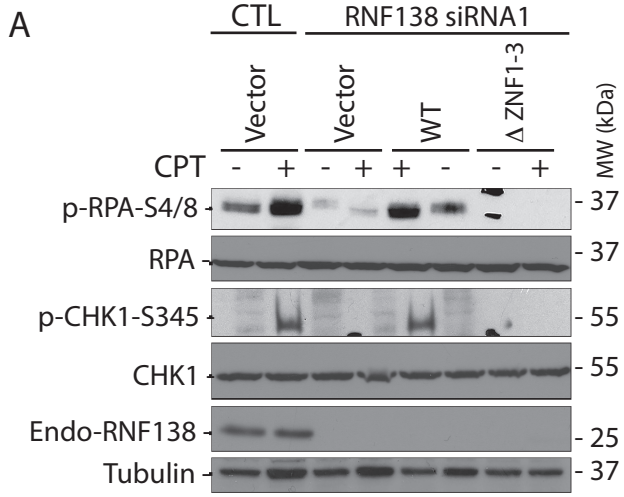
A
CTL
RNF138 siRNA1
Vector
Vector
WT
Δ ZNF1-3
CPT - + - + + - - +
MW (kDa)
p-RPA-S4/8
RPA
p-CHK1-S345
CHK1
Endo-RNF138
Tubulin
37
37
55
55
25
37

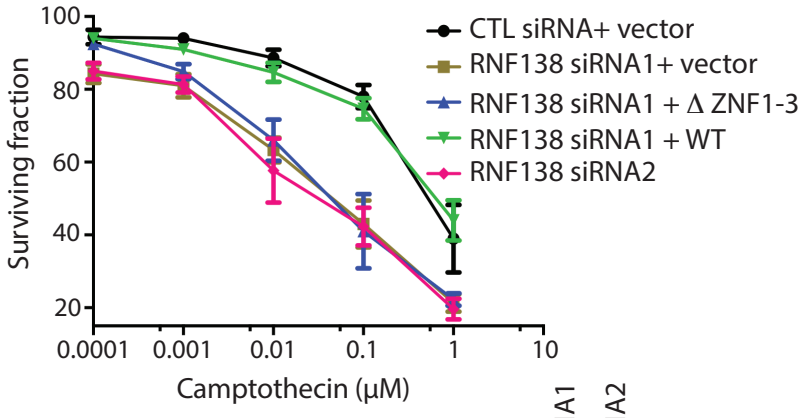
B
Surviving fraction
100
80
60
40
20
0.0001
0.001
0.01
0.1
1
10
Camptothecin (μM)
CTL siRNA+ vector
RNF138 siRNA1+ vector
RNF138 siRNA1 + Δ ZNF1-3
RNF138 siRNA1 + WT
RNF138 siRNA2

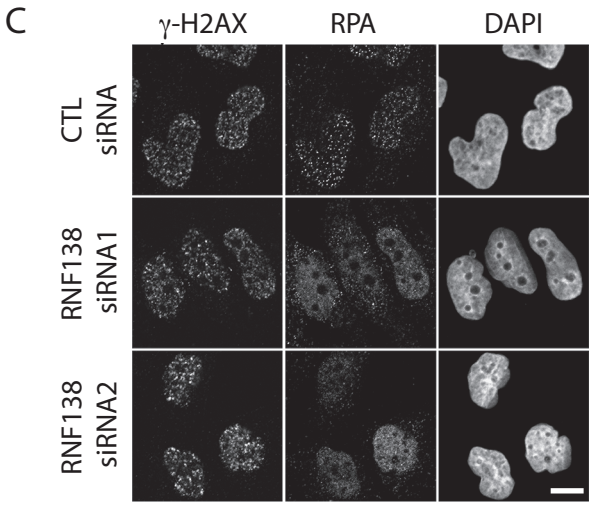
C
γ-H2AX
RPA
DAPI
CTL siRNA
RNF138 siRNA1
RNF138 siRNA2

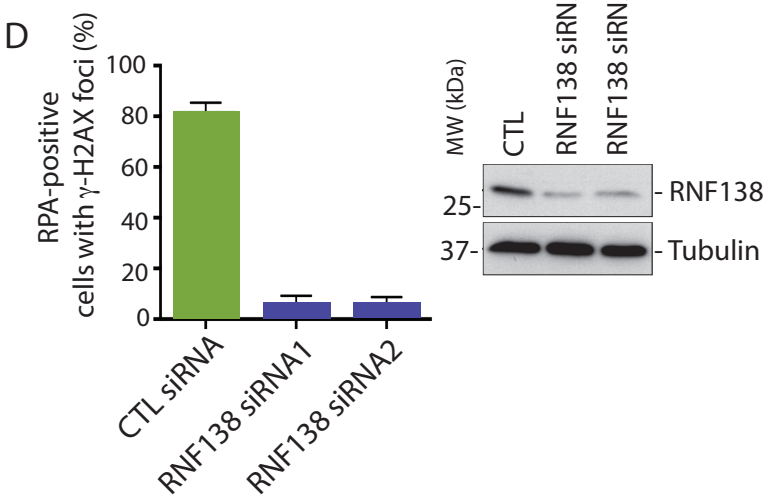
D
RPA-positive cells with γ-H2AX foci (%)
100
80
60
40
20
0
CTL siRNA
RNF138 siRNA1
RNF138 siRNA2
MW (kDa)
CTL
RNF138 siRNA1
RNF138 siRNA2
25-
37-
RNF138
Tubulin

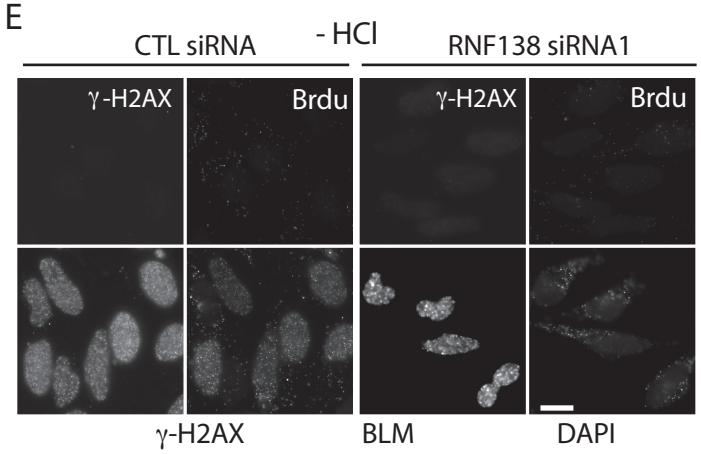
E
CTL siRNA
- HCl
RNF138 siRNA1
γ-H2AX
Brdu
γ-H2AX
Brdu
No IR
IR

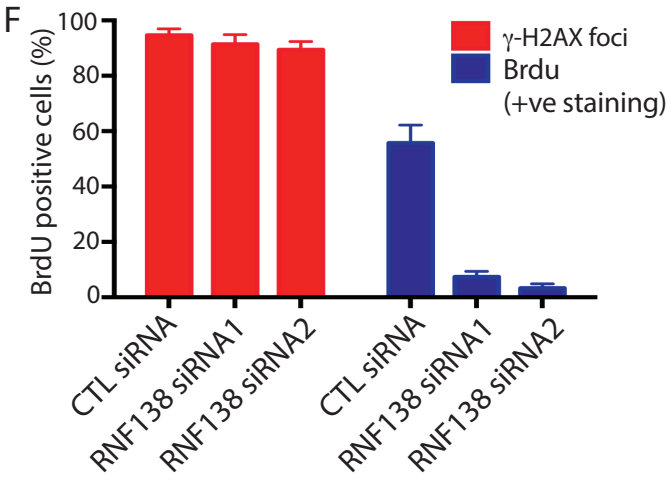
F
BrdU positive cells (%)
100
80
60
40
20
0
γ-H2AX foci
Brdu
(+ve staining)
CTL siRNA
RNF138 siRNA1
RNF138 siRNA2
CTL siRNA
RNF138 siRNA1
RNF138 siRNA2

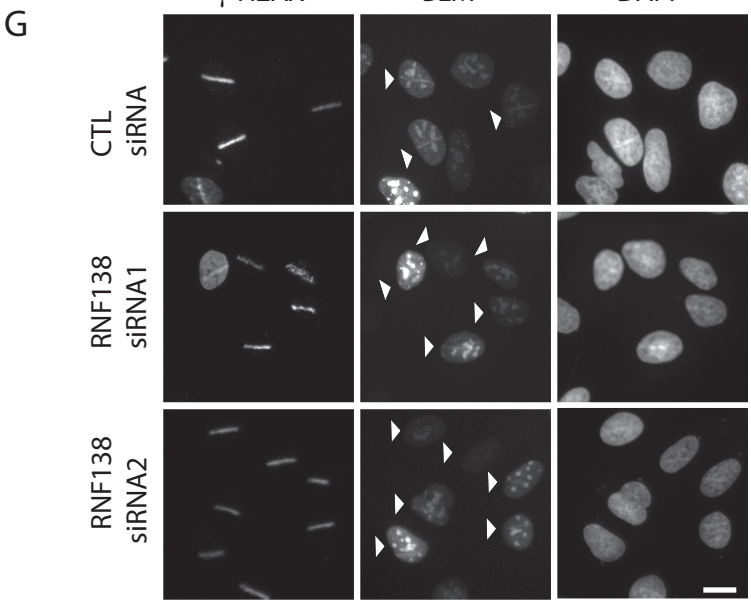
G
γ-H2AX
BLM
DAPI
CTL siRNA
RNF138 siRNA1
RNF138 siRNA2

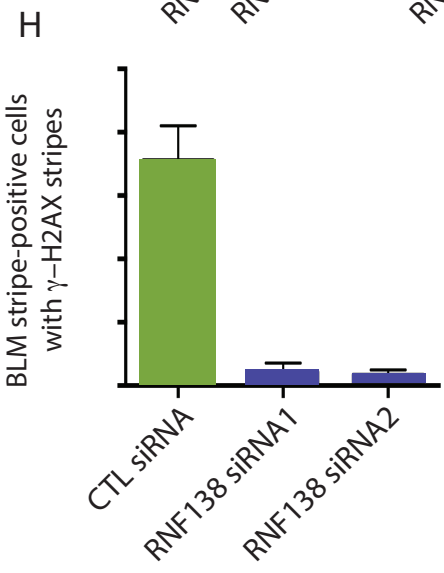
H
BLM stripe-positive cells with γ–H2AX stripes
CTL siRNA
RNF138 siRNA1
RNF138 siRNA2

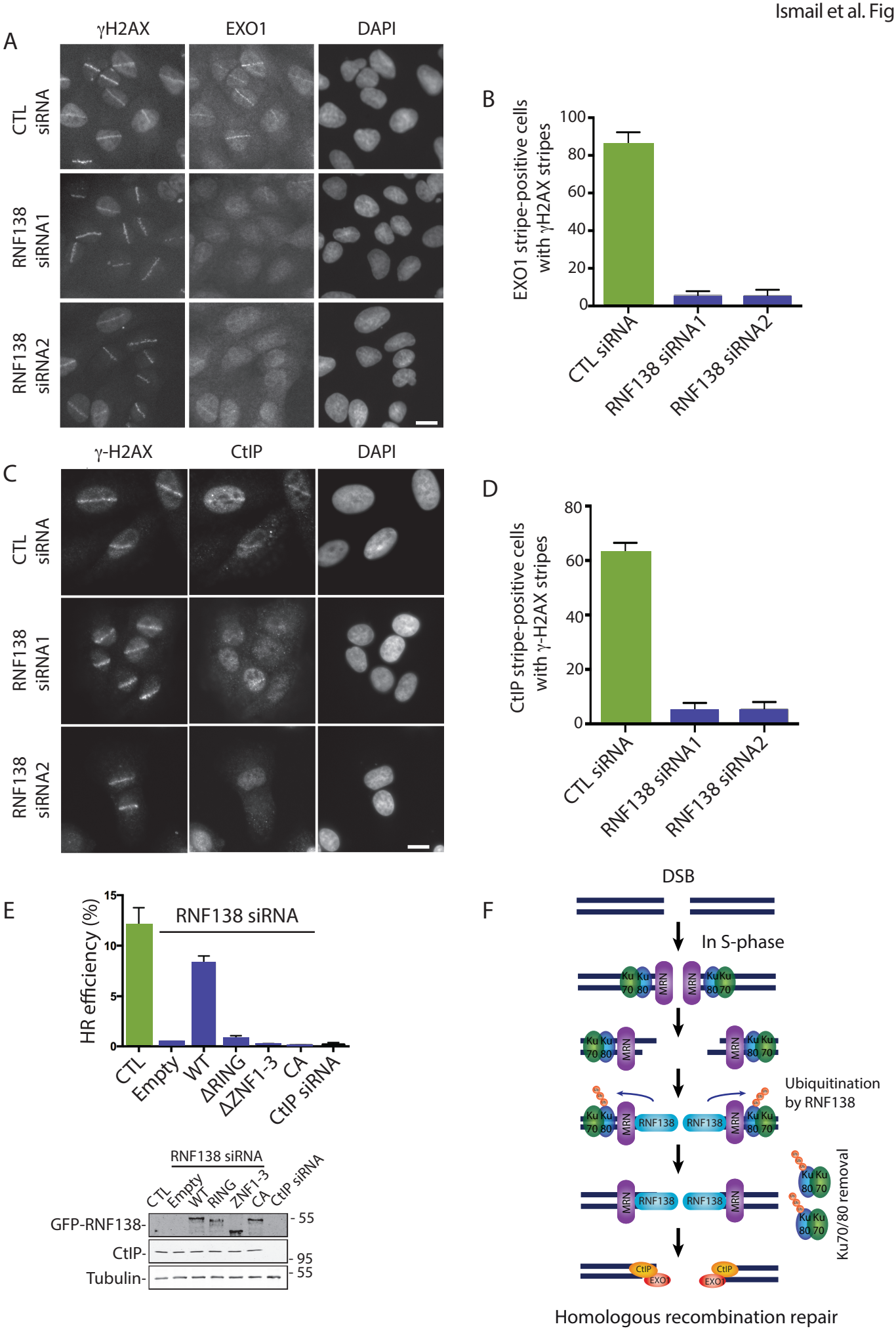
A
γH2AX
EXO1
DAPI
CTL siRNA
RNF138 siRNA1
RNF138 siRNA2
B
EXO1 stripe-positive cells with γH2AX stripes
100
80
60
40
20
0
CTL siRNA
RNF138 siRNA1
RNF138 siRNA2
C
γ-H2AX
CtIP
DAPI
CTL siRNA
RNF138 siRNA1
RNF138 siRNA2
D
CtIP stripe-positive cells with γ-H2AX stripes
80
60
40
20
0
CTL siRNA
RNF138 siRNA1
RNF138 siRNA2
E
HR efficiency (%)
15
10
5
0
RNF138 siRNA
CTL
Empty
WT
ΔRING
ΔZNF1-3
CA
CtIP siRNA
RNF138 siRNA
CTL
Empty
WT
RING
ZNF1-3
CA
CtIP siRNA
GFP-RNF138-
CtIP-
Tubulin-
55
95
55
F
DSB
In S-phase
Ku 70 80
MRN
Ubiquitination by RNF138
RNF138
Ku70/80 removal
CtIP
EXO1
Homologous recombination repair

## Online Methods

### Cell culture, antibodies, and plasmids

The NHEJ reporter construct 'sGEJ' was kindly provided by Dr. Ralph Scully[38]and stably integrated into the genomic DNA of MCF-7 cells by using G418 disulphate salt (400 μg/ml; Sigma) as a selection marker. The HR reporter construct 'DR-GFP' (kindly provided by Dr. Maria Jasin)[39] was integrated into the genomic DNA of MCF-7 cells by hygromycin selection (400 μg/ml; Invitrogen). Human U2OS, U2OS cell stably expressing GFP-Exo1, GFP-CtIP (kindly provided by Dr. Steve Jackson), GFP-BLM and GFP-RAD52/RFP-H2B were cultured in DMEM by G418 selection (500 μg/ml; Invitrogen), while MCF-7 cells were cultured in MEM-alpha (air/$CO_2$, 19:1, 37°C). Both media were supplemented with 10% fetal bovine serum. List of all antibodies used in the study are summarized in **Supplementary Table 3**. The full-length and deletion/point mutants of human RNF138 were generated by PCR and subcloned into the eGFP-C1 vector (Invitrogen). List of all PCR primers used in the study are summarized in **Supplementary Table 4**. To measure Ku80 degradation, cells were treated with cycloheximide (40 μg/mL) and MG132 (20 μM). All siRNA duplexes were purchased from IDT or Dharmacon. List of all siRNA used in the study are summarized in **Supplementary Table 5**. Cell transfections with plasmid DNA or siRNA duplexes were performed by using Effectene® (Qiagen) and/or Lipofectamine 3000 and Lipofectamine RNAiMax (Invitrogen), respectively, following the manufacturer's instructions. KU-55933 (ATM inhibitor) and Mirin (Mre11 inhibitor) were purchase from Selleckchem and Sigma respectively,

dissolved in DMSO, and kept in aliquots

at -80 C.

**NHEJ and HR assays**

$1\times10^6$ cells stably expressing the GFP-reporter system were transfected with control or one of two different RNF138 siRNA for 24 hr. Cells were then electroporated with 10 μg of pCBASce plasmid at 270V, 975uF using a BioRad Genepulsar II. Cells were plated onto 10 cm dishes and incubated in culture media for forty-eight hours prior to FACS analyses. Results were the averages of data obtained from three independent experiments.

**Cell survival assays**

$1\times10^3$ cells that were transfected with control or one of two different RNF138 siRNA were seeded onto 60 mm dish in triplicate. Twenty-four hours after transfection, cells were treated with CPT or irradiated. Medium was replaced twenty-four hours later and cells were then incubated for fourteen days. Resulting colonies were stained with 0.5% crystal violet/20% ethanol and counted. Results were normalized to plating efficiencies. The colonies were counted and results were presented as the averages of data obtained from three independent experiments.

**Biochemical cell fractionation and immunoblot analysis**

Cell fractionation of mammalian cells was performed essentially as described[40]. Approximately $3 \times 10^6$ cells were washed in PBS and resuspended in 200 μl of solution A (10 mM HEPES [pH 7.9], 10 mM KCl, 1.5 mM $MgCl_2$, 0.34 M sucrose, 10%

glycerol, 1 mM DTT, protease and phosphatase inhibitors (life technologies)). Triton X-100 was added to a final concentration of 0.1%, cells were incubated on ice for 5 min, and the cytoplasmic (Cyto) and nuclear fractions were harvested by centrifugation at 1,300 × g for 4 min. Isolated nuclei were then washed in solution A, lysed in 150 µl solution B (3 mM EDTA, 0.2 mM EGTA, 1 mM DTT, protease and phosphatase inhibitors), and incubated on ice for 10 min. The soluble nuclear (Nucl) and chromatin fractions were harvested by centrifugation at 1,700 × g for 4 min. Isolated chromatin (Chr) was then washed in solution B, spun down at 10,000 × g, and resuspended in 150 µl Laemmli sample buffer. Proteins were resolved by SDS-PAGE, transferred onto nitrocellulose (BioRad) and probed using the appropriate primary and secondary antibodies (a full list of antibodies can be found in supplementary table 1). Secondary antibodies were conjugated with infrared specific dyes (either Alexa Fluor® 680 or Alexa Fluor® 750 or IRDye® 800), and fluorescence was imaged on the Odyssey Infrared Imaging system (LiCor Biosciences). For detection of endogenous ubiquitylated Ku80 following DNA damage, the membrane was denatured after transfer in a 6M guanidine-HCL solution (6M guanidine-HCL, 20 mM Tris-HCL pH 7.5, 1 mM PMSF, 5 mM DTT) for 30 minutes at room temperature. Polyubiquitylation signal was detected using an anti-ubiquitin monoclonal antibody (Santa-Cruz Biotechnology, Santa-Cruz, CA, USA).

**Purification of recombinant proteins**

RNF138 WT, mutant C18A/C54A and mutant ΔZNF1-3 were purified from baculovirus-infected Sf9 cells as described in[41]. Insect cells were infected with a dilution 1: 100 for 60 hours.

**Electrophoretic Mobility Shift Assay (EMSA)**

DNA substrates were made by the annealing of the primer JYM698 for DS, JYM699 for 3'-tail and JYM697 for 5'-tail with the $^{32}$P-labeled primer JYM696 (List of all DNA EMSA probes can be found in **Supplementary Table 6**). Reactions (10 µL) contained 50 nM of $^{32}$P-labelled DNA oligonucleotides and the protein at the indicated concentrations in binding buffer (25 mM MOPS (morpholine-propanesulfonic acid) pH 7.0, 0.2% Tween-20, 1 mM $CaCl_2$ and 2 mM DTT). Proteins were added to reactions and incubated at 37°C for 10 minutes, followed by 15 minutes of fixation with 0.2% glutaraldehyde. Reactions were loaded onto an 8% TBE 1X acrylamide gel and run at 150V during 60 minutes.

**Live-cell microscopy and laser micro-irradiation**

Cells grown on coverslips were incubated with 0.5 µg/ml Hoechst 33342 for 15 min and then placed on the stage of a Zeiss LSM510 NLO laser-scanning confocal microscope. DSBs were generated as previously described[42] using a near-infrared 750 nm titanium-sapphire laser line. The laser output was set to 5–10% (unless stated otherwise), and we used 10 iterations to generate localized DSBs with a Plan-Neofluar 40×/1.3 N.A. oil immersion objective. For immunofluorescence staining of micro-irradiated cells, cells were permitted to recover in a 37°C humidified

incubator containing 5% $CO_2$ for the indicated times post damage before 4% paraformaldehyde fixation and indirect immunofluorescent staining as detailed above.

**Immuofluorescence staining**

IR or laser-irradiated cells were analysed by immunofluorescence for the effect of RNF138 knock down on the localization of different DNA repair proteins at sites of IR-induced or laser-induced damage using methods that we have described previously[42]. Ku foci immunostaining was done as previously described using RNAase containing extraction buffer[43]. For non-denatured BrdU/RPA immunodetection, cells were pre-extracted twice with BrdU buffer (20 mM HEPES, pH 7.9, 50 mM NaCl, 300 mM Sucrose, 3 mM $MgCl_2$, 0.5% Triton X-100) for 5 minutes before being fixed at the indicated time points after exposing cells to IR or laser microirradiation. Cells were fixed with 4.0% paraformaldehyde in PBS, pH 7.5, for 20 minutes at room temperature. BrdU antibody was incubated overnight at 4 $^{o}$C. Cells were then immunostained as previously described[42].

**Immunoprecipitation**

Cells harvested in PBS were lysed in 20 mM Tris pH 7.5, 150 mM NaCl, 2 mM $MgCl_2$, 0.5% NP-40, 50 U/ml benzonase, supplemented with protease and phosphatase inhibitors. After benzonase treatment for 30 min, the salt concentration was adjusted to 500 mM and cell extracts were further incubated for 15 min on ice. Lysates were clarified by centrifugation (14000 rpm, 15 min, 4°C) and at least 1 mg proteins was used per immunoprecipitation in IP buffer (25 mM Tris pH 7.5, 150

mM NaCl, 1.5 mM DTT, 10% glycerol, 0.5% NP-40) supplemented with protease and phosphatase inhibitors. Endogenous proteins were captured onto protein magnetic Dynabeads (Life Technologies) coupled to the indicated antibody, while GFP/Flag-tagged proteins were captured onto GFP-Trap agarose beads (ChromoTek). Complexes were extensively washed in IP buffer with salt concentration adjusted to 500 mM NaCl. All extracts were pre-cleared using beads alone.

**Chromatin fractionation *and in vivo* Ku ubiquitylation**

To isolate the soluble and chromatin enriched fractions, cells were rinsed twice in cold PBS, incubated for 5 min on ice with gentle shaking in extraction buffer (25 mM HEPES [pH 7.4], 50 mM NaCl, 1 mM EDTA, 3 mM $MgCl_2$, 300 mM sucrose, and 0.5% Triton X-100) and protease inhibitors. After removal of the supernatant (Sol), the cell pellet was re-suspended in the extraction buffer containing 50 U/ml Benzonase® Nuclease (Sigma) and supplemented with EDTA-free protease inhibitors (Roche) incubated on ice for 30 min. Lysates were adjusted to 0.5 M NaCl and incubated on ice for 15 min and cleared of debris by centrifugation at 4°C. Supernatant was collected (Chr). IP of GFP-Ku80 or endogenous Ku80 from the soluble and chromatin fractions was carried out with GFP-Trap beads (ChromoTek) or Ku80 antibody for 3 hrs at 4°C. IP of endogenous ubiquitylated proteins were done using ubiquitin antibody. Beads were washed four times in extraction buffer containing 0.5 M NaCl and subjected to SDS-PAGE and immunoblotting.

**ChIP assay**

The impact of RNF138 knock down on DNA repair protein recruitment to a defined *I-SceI* DSB was determined by ChIP and PCR. Induction of a site specific DSB was performed as described previously[44]. RNF138 enrichment at the FOk1-induced DSBs were done using the FOk1 reporter cells as previously described[45]. Primer sequences can be found in the **supplementary Table 4**.

**Quantitation of RAD52 foci by high content microscopy**

Custom RNAi library targeting bioinformatically collated RING, HECT, and U-box-containing E3 ubiquitin ligases was purchased from Dharmacon. U2OS cells stably expressing GFP-RAD52 and RFP-H2B were used. RNAi screening was used at 25 nM final concentrations and RNAi were reverse transfected with RNAiMAX™ reagent (Life Technologies) in 96-well microscopy plates (μClear, Greiner). After 48 hrs, cells were washed three times with full media and were treated with CPT (1 μM) for 3 hrs at 37$^{o}$C. Cells were fixed with 4% paraformaldehyde for 20 min at room temperature. Individual wells were then mounted in PBS buffer and 96 wells plates were loaded into MD ImageXpress Micro screening microscope equipped with a 20 × 0.5 N.A Fluor dry objective (Nikon). GFP-RAD52 foci were detected in the GFP channel, and cell nuclei were calculated for each of these objects in the RFP channel. Multiple fields of view with two signal channels per field were collected per well of a 96-wells plate, corresponding on average to ~40-200 nuclei per field. Approximately 2000 to 3000 nuclei were analyzed per condition, per imaging experiment. Image segmentation was performed with the ImageXpress software.

For every field of view collected, nuclei (defined by RFP-H2B) and GFP-RAD52 foci were defined and measured using image data captured by the respective CCD cameras dedicated to the 561 or 488 nm laser light sources. Partial nuclei were discarded from analysis. Nuclear borders were overlaid onto GFP fluorescence image data, and RAD52 foci signal was restricted to these nuclear zones. RAD52 foci were detected using a spot finding algorithm and values describing the number and size of RAD52 foci were obtained. The percentage of cells having more than 50 foci per cell is calculated using a script written in excel.

**Assessment of *Z*-scores for siRNAs**

To score siRNAs during the primary screen according to their potency in affecting RAD52 focus formation, we ranked each duplicate transfection according to their z-score (*Z*), which allowed correcting for plate-to-plate variations. For each RNAi we derived a population mean X and standard deviation σ. To center X around the non-targeting control (ctr) we calculated an adjustment factor alpha = median(X_ctr)/sd(X_ctr) and

used the non-targeting control as follows:

$$Z = \frac{(x - \mu) * \alpha}{\sigma}$$

where μ = is the median non-targeting control between wells per plate and σ = the standard deviation of the sample population of X.

**PAR polymer-blot analysis**

Purified recombinant human RNF138 was tested for its ability to bind PAR. Bovine serum albumin (BSA) and purified Hela core histones (Active Motif) were respectively used as negative and positive PAR-binding controls. One microgram of each protein was prepared in 150 µL of TBS-T buffer (10 mM Tris-HCl pH 8.0, 150 mM NaCl and 0.1% Tween-20) prior to being slot-blotted on 0.2 µM pore size nitrocellulose membrane using a Bio-Dot® microfiltration apparatus (Bio-Rad). A Ponceau staining of proteins on nitrocellulose membrane was performed to confirm uniform transfer of proteins. Although proteins were blotted in their native form, the blot was incubated for 1h in TBS-T containing 10 mM β-mercaptoethanol to favor proper protein folding. Then, the membrane was incubated for 1h in TBS-T buffer containing 250 nM of Dihydroxyboronyl Bio-Rex (DHBB)-purified $^{32}$P-labeled PAR synthesized as described in [46]. The membranes were rinsed several times with TBS-T until no radioactivity could be detected in the washes. Subsequently, the membranes were air-dried, subjected to autoradiography and analyzed on a Typhoon phosphorimager system (GE Healtcare).

**Protein in-gel digestion**

After brief separation by SDS-PAGE (~ 1 cm below the bottom of the wells) and SYPRO staining, the resulting gel lanes were extracted, placed in 96-well plates and then washed with water. Tryptic digestion was performed on a MassPrep liquid handling workstation (Waters, Milford, USA) according to the manufacturer's specifications and to the protocol of Shevchenko *et al* [47] with the modifications

suggested by Havlis **et al** [48]. Briefly, proteins were reduced with 10 mM DTT and alkylated with 55 mM iodoacetamide. Trypsin digestion was performed using 126 nM of modified porcine trypsin (Sequencing grade, Promega, Madison, WI) at 58°C for 1h. Digestion products were extracted using 1% formic acid, 2% acetonitrile followed by 1% formic acid, 50% acetonitrile. The recovered extracts were pooled, vacuum centrifuge dried and then resuspended into 7 µl of 0.1% formic acid and 2 µl were analyzed by mass spectrometry.

**LC-MS/MS**

Mass spectrometry analysis was performed on a TripleTOF® 5600 mass spectrometer fitted with a nanospray III ion source (ABSciex, Concord, ON) and coupled to an Agilent 1200 HPLC. Samples were injected by the Agilent 1200 autosampler onto a 0.075 mm (internal diameter) self-packed PicoFrit column (New Objective) packed with a isopropanol slurry of 5 µm Jupiter C18 (Phenomenex) stationary phase using a pressure vessel set at 700 p.s.i . The length of the column was 15 cm. Samples were run using a 65 min gradient from 5-35% solvent B (solvent A 0.1% formic acid in water; solvent B: 0.1% formic acid in acetonitrile) at a flow rate of 300 nl/min. Data was acquired using an ion spray voltage of 2.4kV, curtain gaz of 30 PSI, nebulizer gaz of 8 PSI an an interface heater temperature of 125 ºC. An information-dependant acquisition (IDA) method was set up with the MS survey range set between 400 and 1250 amu (250 msec) followed by dependent MS/MS scans with a mass range set between 100 and 1800 amu (50 msec) of the 20 most intense ions in the high sensitivity mode with 2+ to 5+ charge state. Dynamic

exclusion was set for a period of 3 sec and a tolerance of 100 ppm. MGF peak list files were created using Protein Pilot version 4.5 (ABSciex) utilizing the Paragon and Progroup algortihms [49].

**Database searching**

All MS/MS samples were analyzed using Mascot (Matrix Science, London, UK; version 2.4.1) and X! Tandem (The GPM, thegpm.org; version CYCLONE (2010.12.01.1)). Mascot was set up to search the Uniprot database (2014-05-12, 69 138 entries) assuming the digestion enzyme trypsin. X! Tandem was set up to search a subset of the same database also assuming trypsin. Mascot and X! Tandem were searched with a fragment ion mass tolerance of 0,100 Da and a parent ion tolerance of 0,100 Da. Carbamidomethyl of cysteine was specified in Mascot and X! Tandem as a fixed modification. Glu->pyro-Glu of the n-terminus, ammonia-loss of the n-terminus, gln->pyro-Glu of the n-terminus, oxidation of methionine, acetyl of the n-terminus, phosphorylation of serine and threonine and GlyGly of lysine were specified in X! Tandem as variable modifications. Oxidation of methionine, acetyl of the n-terminus, phosphorylation of serine and threonine, GlyGly of lysine and LeuArgGlyGly of lysine were specified in Mascot as variable modifications.

**Criteria for protein identification**

Scaffold (version Scaffold_4.2.0, Proteome Software Inc., Portland, OR) was used to validate MS/MS based peptide and protein identifications. Peptide identifications were accepted if they could be established at greater than 87,0 % probability to achieve an FDR less than 1,0 % by the Scaffold Local FDR algorithm [50] . Protein

identifications were accepted if they could be established at greater than 99,0 % probability to achieve an FDR less than 1,0 % and contained at least 2 identified peptides. Protein probabilities were assigned by the Protein Prophet algorithm [51]. Proteins that contained similar peptides and could not be differentiated based on MS/MS analysis alone were grouped to satisfy the principles of parsimony.

## References


38. Xie, A., Kwok, A. & Scully, R. Role of mammalian Mre11 in classical and alternative nonhomologous end joining. *Nature structural & molecular biology* **16**, 814-818 (2009).
39. Pierce, A.J., Johnson, R.D., Thompson, L.H. & Jasin, M. XRCC3 promotes homology-directed repair of DNA damage in mammalian cells. *Genes & development* **13**, 2633-2638 (1999).
40. Mendez, J. & Stillman, B. Chromatin association of human origin recognition complex, cdc6, and minichromosome maintenance proteins during the cell cycle: assembly of prereplication complexes in late mitosis. *Molecular and cellular biology* **20**, 8602-8612 (2000).
41. Maity, R. *et al.* GST-His purification: a two-step affinity purification protocol yielding full-length purified proteins. *Journal of visualized experiments : JoVE*, e50320 (2013).
42. Ismail, I.H. *et al.* CBX4-mediated SUMO modification regulates BMI1 recruitment at sites of DNA damage. *Nucleic acids research* (2012).
43. Britton, S., Coates, J. & Jackson, S.P. A new method for high-resolution imaging of Ku foci to decipher mechanisms of DNA double-strand break repair. *The Journal of cell biology* **202**, 579-595 (2013).
44. Rodrigue, A. *et al.* Interplay between human DNA repair proteins at a unique double-strand break in vivo. *The EMBO journal* **25**, 222-231 (2006).
45. Shanbhag, N.M., Rafalska-Metcalf, I.U., Balane-Bolivar, C., Janicki, S.M. & Greenberg, R.A. ATM-dependent chromatin changes silence transcription in cis to DNA double-strand breaks. *Cell* **141**, 970-981 (2010).
46. Menard, L. & Poirier, G.G. Rapid assay of poly(ADP-ribose) glycohydrolase. *Biochem Cell Biol* **65**, 668-673 (1987).
47. Shevchenko, A., Wilm, M., Vorm, O. & Mann, M. Mass spectrometric sequencing of proteins silver-stained polyacrylamide gels. *Analytical chemistry* **68**, 850-858 (1996).
48. Havlis, J., Thomas, H., Sebela, M. & Shevchenko, A. Fast-response proteomics by accelerated in-gel digestion of proteins. *Analytical chemistry* **75**, 1300-1306 (2003).

49. Shilov, I.V. *et al.* The Paragon Algorithm, a next generation search engine that uses sequence temperature values and feature probabilities to identify peptides from tandem mass spectra. *Mol Cell Proteomics* **6**, 1638-1655 (2007).
50. Keller, A., Nesvizhskii, A.I., Kolker, E. & Aebersold, R. Empirical statistical model to estimate the accuracy of peptide identifications made by MS/MS and database search. *Anal Chem* **74**, 5383-5392 (2002).
51. Nesvizhskii, A.I., Keller, A., Kolker, E. & Aebersold, R. A statistical model for identifying proteins by tandem mass spectrometry. *Anal Chem* **75**, 4646-4658 (2003).